Article

QUANTUM SPIN-WAVE THEORY FOR NON-COLLINEAR SPIN STRUCTURES, A REVIEW

Hung T. Diep *

Laboratoire de Physique Théorique et Modélisation, CY Cergy Paris Université[1], CNRS, UMR 8089
2 Avenue Adolphe Chauvin, 95302 Cergy-Pontoise, France
* Correspondence: diep@cyu.fr

Received: date; Accepted: date; Published: date

Abstract: In this review, we trace the evolution of the quantum spin-wave theory treating non-collinear spin configurations. Non-collinear spin configurations are consequences of the frustration created by competing interactions. They include simple chiral magnets due to competing nearest-neighbor (NN) and next-NN interactions and systems with geometry frustration such as the triangular antiferromagnet and the Kagomé lattice. We review here spin-wave results of such systems and also systems with the Dzyaloshinskii-Moriya interaction. Accent is put on these non-collinear ground states which have to be calculated before applying any spin-wave theory to determine the spectrum of the elementary excitations from the ground states. We mostly show results from a self-consistent Green'function theory to calculate the spin-wave spectrum and the layer magnetizations at finite T in two and three dimensions as well as in thin films with surface effects. Some new unpublished results are also included. Analytical details and the validity of the method are shown and discussed.

Keywords: Quantum Spin-Wave Theory; Frustrated Spin Systems ; Non-Collinear Spin Configurations; Dzyaloshinskii-Moriya Interaction; Phase Transition; Green's Function Theory; Monte Carlo Simulation

1. Introduction

In a solid the interaction between its constituent atoms or molecules gives rise to elementary excitations from its ground state (GS) when the temperature increases from zero. One has examples of elementary excitations due to atom-atom interaction known as phonons or due to spin-spin interaction known as magnons. Note that magnons are spin waves (SW) when they are quantized. Elementary excitations are defined also for interaction between charge densities in plasma, or for electric dipole-dipole interaction in ferroelectrics, among others. Elementary excitations are thus collective motions which dominate the low-temperature behaviors of solids in general.

For a given system, there are several ways to calculate the energy of elementary excitations from classical treatments to quantum ones. Since those collective motions are waves, its energy depends on the wave vector **k**. The **k**-dependent energy is often called the SW spectrum for spin systems. Note that though the calculation of the SW spectrum is often for periodic crystalline structures, it can also be performed for symmetry-reduced systems such as in thin films or in semi-infinite solids in which the translation symmetry is broken by the presence of a surface.

In this review we focus on the SW excitations in magnetically ordered systems. The history began with ferromagnets and antiferromagnets with collinear spin GSs, parallel or antiparallel configurations in the early 50's. Most of the works on the SW used either the classical method or the quantum Holstein-Primakoff transformation. The Green's function (GF) technique has also been introduced in a

*diep@cyu.fr
1 Formerly, University of Cergy-Pontoise

 doi:10.20944/preprints202207.0268.v1

pioneer paper of Zubarev [1]. The first application of this method to thin films has been done [2]. Note that unlike the SW theory, the GF can treat the SW up to higher temperatures. We will come back to this point later.

Let us recall some important breakthroughs in the study of in non-collinear spin configurations. The first discovery of the helical spin configuration has been published in 1959 [3,4]. Some attempts to treat this non-collinear case have been done in the 70's and 80's. Let us cite two noticeable works on this subject in Refs. [5,6]. In these works, a local system of spin coordinates have been introduced in the way that each spin lies on its quantization axis. One can therefore use the commutation relations between spin deviation operators. These works took into account magnon-magnon interactions by expanding the Hamiltonian up to three-operator terms at temperature $T = 0$ [5] or up to four-operator terms at low T [6]. Nevertheless, since these works used the Holstein-Primakoff method, the case of higher T cannot be dealt with. In Ref. [7], the GF method has been employed for the first time to calculate the SW spectrum in a frustrated system where the GS spin configuration is non collinear. Using the SW spectrum, the local order parameter, the specific heat, ... were calculated. Since this work, we have applied the GF method to a variety of systems where the GS is non collinear. In this review, we will recall results of some of these published works.

Let us comment on the frustration which is the origin of the non-collinear GS. The frustration is caused by either the competing interactions in the system or a geometry frustration as in the triangular lattice with only the antiferromagnetic interaction between the nearest neighbors (NN) (see Ref. [8]). The frustration causes high GS degeneracy, and in the case of XY and Heisenberg spins the GS is non collinear making the calculation of the SW spectrum harder. A number of examples will be shown in this review paper.

In addition to competing interactions, the Dzyaloshinskii-Moriya (DM) interaction [9,10] is also the origin of non-collinear spin configurations in spin systems. While the Heisenberg model between two spins is written as $-J_{ij}\mathbf{S}_i \cdot \mathbf{S}_j$ giving rise to two collinear spins in the GS, the DM interaction is written as $\mathbf{D}_{ij} \cdot \mathbf{S}_i \times \mathbf{S}_j$ giving rise to two perpendicular spins. The DM model was historically proposed to explain the weak ferromagnetism which was observed in Mn compounds [11]. However, the DM interaction goes beyond the weak magnetism since it was discoververed in various materials, in particular at the interface of a multilayer [12–16]. Although in this review we do not show the effect of the DM interaction in a magnetic field which gives rise to topological spin swirls known as skyrmions, we should mention a few of the important works given in Refs. [17–20]. Skyrmions are among the most studied subjects at the time being due to their potental applications in spinelectronics.[22] We refer the reader to the rich biography given in our recent papers in Refs. [23,24].

Since this paper is a review on the method and the results of published works on SW in non-collinear GS spin configurations, it is important to recall the method and show main results of some typical cases. We would like to emphasize that on the GF technique, to our knowledge there are no authors other than us working with this method. Therefore, the works mentioned in the references of this paper are our works published over the last 25 years. The aim of this review is two-fold. First we show technical details of the GF method by selecting a number of subjects which are of current interest in research: helimagnets, systems including a DM interaction, surface effects in thin films. Second, we show that these systems possess many striking features due to the frustration.

This paper is organized as follows. In section 2, we express the Hamiltonian in a general non-collinear GS and define the local system of spin coordinates. Here, we also present the determination of the GS and the formulation of the self-consistent GF method and the calculation of the SW spectrum and layer magnetizations at finite temperature (T). We show in section 3 the numerical results obtained from the GF. Section 4 shows interesting examples using various kinds of interaction including the DM interaction in a variety of systems from two dimensions, to thin films and superlattices. Section 5 treats a case where the DM interaction competes with the antiferromagnetic interaction in the frustrated antiferromagnetic triangular lattice. Section 6 presents the surface effect in a thin film where its surface is frustrated. Concluding remarks are given in section 7.

Preprints (www.preprints.org) | NOT PEER-REVIEWED | Posted: 18 July 2022 doi:10.20944/preprints202207.0268.v1

2. Hamiltonian of a Chiral Magnet - Local Coordinates

Chiral order in helimagnets has been subject of recent extensive investigations. In Ref. [25], the magnetic surface phase of thin helimagnetic films has been studied. In Ref. [26] exotic magnetic structures in ultrathin helimagnetic holmium films have been investigated. In Refs. [27,28] chiral modulation and reorientation effects in MnSi thin films have been theoretically studied. In these works, the chiral structures have been considered at $T = 0$, but not the SW even at $T = 0$. The main difficulty was due to the non-collinear, non-uniform spin configurations. We have shown that this was possible using the GFs generalized for such spin configurations given in Ref. [7]

To demonstrate the method, let us follow Ref. [29]: we consider the body-centered tetragonal (bct) lattice with Heisenberg spins interacting with each other via J_1 the interaction between nearest neighbors (NN) and J_2 the interaction between the next NN (NNN) only in the c-direction (see Fig.1).

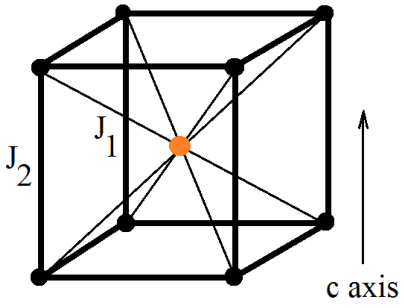

Figure 1. Interactions J_1 (thin solid lines) between NN and J_2 between NNN along the c axis in a bct lattice.

We consider the simplest model of helimagnet given by the following Hamiltonian

$$\mathcal{H} = -J_1 \sum_{i,j} \mathbf{S}_i \cdot \mathbf{S}_j - J_2 \sum_{i,k} \mathbf{S}_i \cdot \mathbf{S}_k \tag{1}$$

where $\mathbf{S}_i$ is a quantum spin of magnitude $1/2$, the first sum is performed over all NN pairs and the second sum over pairs on the c-axis (cf. Fig. 1).

In the case of an infinite crystal, the chiral state occurs when J_1 is ferromagnetic and J_2 is antiferromagnetic and $|J_2|/J_1$ is larger than a critical value, as will be shown below.

Let us suppose that the energy of a spin E_C in a chiral configuration when the angle between two NN spin in the adjacent planes is θ, one has (omitting the factor S^2)

$$E = -8J_1 \cos\theta - 2J_2 \cos(2\theta) \tag{2}$$

The lowest-energy state corresponds to

$$\begin{aligned} \frac{dE}{d\theta} &= 0 \\ \rightarrow 8J_1 \sin\theta + 4\sin(2\theta) &= 0 \\ 8J_1 \sin\theta(1 + \frac{J_2}{J_1} cos\theta) &= 0 \end{aligned} \tag{3}$$

There are two solutions, $\sin\theta = 0$ and $\cos\theta = -\frac{J_1}{J_2}$ The first solution corresponds to the ferromagnetic state, and the second solution exists if $-\frac{J_1}{J_2} \leq 1$ which corresponds to the chiral state.

Preprints (www.preprints.org) | NOT PEER-REVIEWED | Posted: 18 July 2022 doi:10.20944/preprints202207.0268.v1

For a thin helimagnetic film, the angles between spins in the adjacent layers are not the same due to the surface. We can use the method of energy minimization for each layer, then we have a set of coupled equations to solve (see Ref. [29]). Figure 2 displays an example of the angle distribution across the film thickness N_z.

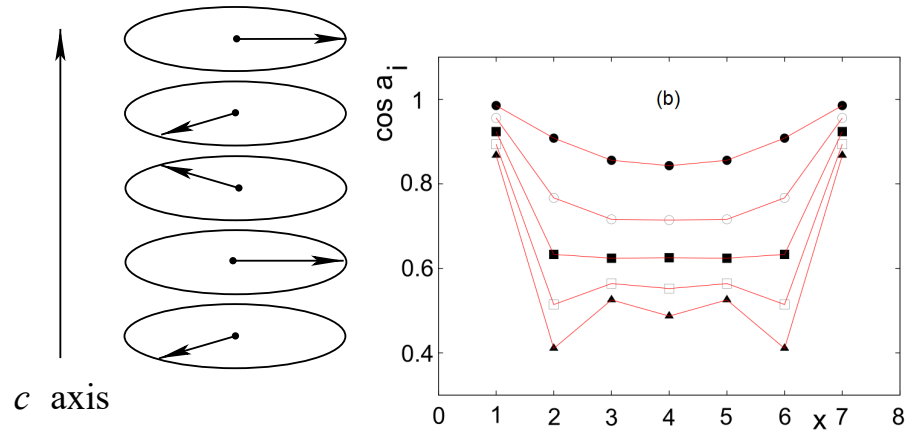

Figure 2. (a) Chiral structure along the c-axis for an infinite crystal, in the case $\theta = 2\pi/3$, namely $J_2/J_1 = -2$; (b) Cosinus of $\alpha_1 = \theta_1 - \theta_2$, ..., $\alpha_7 = \theta_7 - \theta_8$ across the film for several values $J_2/J_1 = -1.2, -1.4, -1.6, -1.8, -2$ (from top) with $N_z = 8$: a_i stands for $\theta_i - \theta_{i+1}$ and x indicates the film layer i where the angle a_i with the layer $(i+1)$ is shown. See text for comments.

In order to calculate the SW spectrum for systems of non-collinear spin configurations, let us emphasize that the commutation relations between spin operators are established when the spin lies on its quantization z. In the non-collinear cases, each spin has its own quantization axis. It is therefore important to choose a quantization axis for each spin. We have to use the system of local coordinates defined as follows. In the Hamiltonian, the spins are coupled two by two. Consider a pair $\mathbf{S}_i$ and $\mathbf{S}_j$. As seen above, in the general case these spins make an angle $\theta_{i,j} = \theta_j - \theta_i$ determined by the competing interactions in the systems. For quantum spins, in the course of calculation we need to use the commutation relations between the spin operators S^z, S^+, S^-. As said above, these commutation relations are derived from the assumption that the spin lies on its quantization axis z. We show in Fig. 3 the local coordinates assigned to spin $\mathbf{S}_i$ and $\mathbf{S}_j$. We write

$$\mathbf{S}_i = S_i^x \hat{\xi}_i + S_i^y \hat{\eta}_i + S_i^z \hat{\zeta}_i \quad (4)$$

$$\mathbf{S}_j = S_j^x \hat{\xi}_j + S_j^y \hat{\eta}_j + S_j^z \hat{\zeta}_j \quad (5)$$

Expressing the axes of $\mathbf{S}_j$ in the frame of $\mathbf{S}_i$ one has

$$\hat{\zeta}_j = \cos\theta_{i,j}\hat{\zeta}_i + \sin\theta_{i,j}\hat{\xi}_i \quad (6)$$

$$\hat{\xi}_j = -\sin\theta_{i,j}\hat{\zeta}_i + \cos\theta_{i,j}\hat{\xi}_i \quad (7)$$

$$\hat{\eta}_j = \hat{\eta}_i \quad (8)$$

so that

$$\mathbf{S}_j = S_j^x(-\sin\theta_{i,j}\hat{\zeta}_i + \cos\theta_{i,j}\hat{\xi}_i) + S_j^y\hat{\eta}_i + S_j^z(\cos\theta_{i,j}\hat{\zeta}_i + \sin\theta_{i,j}\hat{\xi}_i) \quad (9)$$

Preprints (www.preprints.org) | NOT PEER-REVIEWED | Posted: 18 July 2022 doi:10.20944/preprints202207.0268.v1

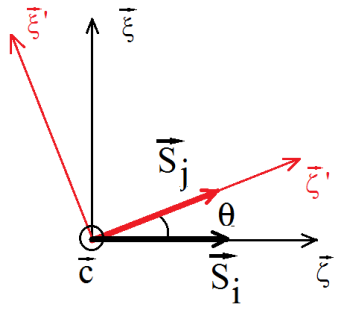

Figure 3. Spin $\mathbf{S}_i$ lies along the $\vec{\zeta}$ axis (its quantization axis), while spin $\mathbf{S}_j$ lies along its quantization axis $\vec{\zeta}'$ which makes an angle θ with the $\vec{\zeta}$ axis. The axes $\vec{\xi}$ and $\vec{\xi}'$ are perpendicular respectively to $\vec{\zeta}$ and $\vec{\zeta}'$. T he perpendicular axes $\hat{\eta}_i$ and $\hat{\eta}_j$ coincide with the $\vec{c}$ axis, perpendicular to the basal plane of the bct lattice.

Using Eq. (9) to express $\mathbf{S}_j$ in the $(\hat{\xi}_i, \hat{\eta}_i, \hat{\zeta}_i)$ coordinates, then calculating $\mathbf{S}_i \cdot \mathbf{S}_j$, we obtain the following exchange Hamiltonian from (28):

$$\begin{aligned}\mathcal{H}_e &= -\sum_{<i,j>} J_{i,j}\Big\{\frac{1}{4}\left(\cos\theta_{i,j}-1\right)\left(S_i^+S_j^+ + S_i^-S_j^-\right)\\ &+ \frac{1}{4}\left(\cos\theta_{i,j}+1\right)\left(S_i^+S_j^- + S_i^-S_j^+\right)\\ &+ \frac{1}{2}\sin\theta_{i,j}\left(S_i^+ + S_i^-\right)S_j^z - \frac{1}{2}\sin\theta_{i,j}S_i^z\left(S_j^+ + S_j^-\right)\\ &+ \cos\theta_{i,j}S_i^zS_j^z\Big\} \qquad (10)\end{aligned}$$

This explicit Hamiltonian in terms of the angle between two NN spins is common for a non-collinear spin configuration due to exchange interactions $J_{i,j}$. For other types of interactions such as the DM interaction, the explicit Hamiltonian in terms of the angle will be different as seen in section 4.

We define the following GFs for the above Hamiltonian:

$$\begin{aligned}G_{i,j}(t,t') &= <<S_i^+(t);S_j^-(t')>>\\ &= -i\theta(t-t')<\left[S_i^+(t),S_j^-(t')\right]> \qquad (11)\\ F_{i,j}(t,t') &= <<S_i^-(t);S_j^-(t')>>\\ &= -i\theta(t-t')<\left[S_i^-(t),S_j^-(t')\right]> \qquad (12)\end{aligned}$$

The equations of motion of these functions are

$$\begin{aligned}i\hbar\frac{d}{dt}G_{i,j}(t,t') &= \left\langle\left[S_i^+(t),S_j^-(t')\right]\right\rangle\delta(t-t')\\ &- \left\langle\left\langle\left[\mathcal{H},S_i^+(t)\right];S_j^-(t')\right\rangle\right\rangle, \qquad (13)\\ i\hbar\frac{d}{dt}F_{i,j}(t,t') &= \left\langle\left[S_i^-(t),S_j^-(t')\right]\right\rangle\delta(t-t')\\ &- \left\langle\left\langle\left[\mathcal{H},S_i^-(t)\right];S_j^-(t')\right\rangle\right\rangle, \qquad (14)\end{aligned}$$

Preprints (www.preprints.org) | NOT PEER-REVIEWED | Posted: 18 July 2022 doi:10.20944/preprints202207.0268.v1

where the spin operators and their commutation relations are given by

$$\begin{aligned} S_j^{\pm} &= S_j^x \hat{\xi}_j \pm i S_j^y \hat{\eta}_j \\ \left[S_j^+, S_l^-\right] &= 2S_j^z \delta_{j,l} \\ \left[S_j^z, S_l^{\pm}\right] &= \pm S_j^{\pm} \delta_{j,l} \end{aligned}$$

Note that the equation of motion of the first function generates functions of the second type, and vice-versa. Expanding the commutators in Eqs. (13)-(14), and using the Tyablikov decoupling scheme [30] for higher-order functions, for example $<< S_{i'}^z S_i^+(t); S_j^-(t') >> \simeq < S_{i'}^z >< < S_i^+(t); S_j^-(t') >>$ etc., we have the following general equations for non-collinear magnets:

$$\begin{aligned} i\hbar \frac{dG_{i,j}(t,t')}{dt} &= 2 < S_i^z > \delta_{i,j}\delta(t-t') \\ &- \sum_{i'} J_{i,i'} [< S_i^z > (\cos\theta_{i,i'} - 1) \times \\ &\times F_{i',j}(t,t') \\ &+ < S_i^z > (\cos\theta_{i,i'} + 1) G_{i',j}(t,t') \\ &- 2 < S_{i'}^z > \cos\theta_{i,i'} G_{i,j}(t,t')] \\ &+ 2 \sum_{i'} I_{i,i'} < S_{i'}^z > \cos\theta_{i,i'} G_{i,j}(t,t') \end{aligned} \tag{15}$$

$$\begin{aligned} i\hbar \frac{dF_{i,j}(t,t')}{dt} &= \sum_{i'} J_{i,i'} [< S_i^z > (\cos\theta_{i,i'} - 1) \times \\ &\times G_{i',j}(t,t') \\ &+ < S_i^z > (\cos\theta_{i,i'} + 1) F_{i',j}(t,t') \\ &- 2 < S_{i'}^z > \cos\theta_{i,i'} F_{i,j}(t,t')] \\ &- 2 \sum_{i'} I_{i,i'} < S_{i'}^z > \cos\theta_{i,i'} F_{i,j}(t,t') \end{aligned} \tag{16}$$

Preprints (www.preprints.org) | NOT PEER-REVIEWED | Posted: 18 July 2022 doi:10.20944/preprints202207.0268.v1

Separating the sums on NN interactions and NNN interactions for the sake of clarity, one has

$$\begin{aligned}
i\hbar\frac{dG_{i,j}(t,t')}{dt} &= 2<S_i^z>\delta_{i,j}\delta(t-t') \\
&- \sum_{k'\in NN} J_{i,k'}[<S_i^z>(\cos\theta_{i,k'}-1)\times \\
&\times F_{k',j}(t,t') \\
&+ <S_i^z>(\cos\theta_{i,k'}+1)G_{k',j}(t,t') \\
&- 2<S_{k'}^z>\cos\theta_{i,k'}G_{i,j}(t,t')] \\
&+ 2\sum_{k'\in NN} I_{i,k'}<S_{k'}^z>\cos\theta_{i,k'}G_{i,j}(t,t') \\
&- \sum_{i'\in NNN} J_{i,i'}[<S_i^z>(\cos\theta_{i,i'}-1)\times \\
&\times F_{i',j}(t,t') \\
&+ <S_i^z>(\cos\theta_{i,i'}+1)G_{i',j}(t,t') \\
&- 2<S_{i'}^z>\cos\theta_{i,i'}G_{i,j}(t,t')] \qquad (17)\\
i\hbar\frac{dF_{k,j}(t,t')}{dt} &= \sum_{i'\in NN} J_{k,i'}[<S_k^z>(\cos\theta_{k,i'}-1)\times \\
&\times G_{i',j}(t,t') \\
&+ <S_k^z>(\cos\theta_{k,i'}+1)F_{i',j}(t,t') \\
&- 2<S_{i'}^z>\cos\theta_{k,i'}F_{k,j}(t,t')] \\
&- 2\sum_{i'\in NN} I_{k,i'}<S_{i'}^z>\cos\theta_{k,i'}F_{k,j}(t,t') \\
&+ \sum_{k'\in NNN} J_{k,k'}[<S_k^z>(\cos\theta_{k,k'}-1)\times \\
&\times G_{k',j}(t,t') \\
&+ <S_k^z>(\cos\theta_{k,k'}+1)F_{k',j}(t,t') \\
&- 2<S_{k'}^z>\cos\theta_{k,k'}F_{k,j}(t,t')] \qquad (18)
\end{aligned}$$

For simplicity, we suppose in the following all NN interactions $(J_{k,k'}, I_{k,k'})$ are equal to (J_1, I_1) and all NNN interactions are equal to J_2. In addition, in the film coordinates defined above, we denote the Cartesian components of the spin position $\mathbf{R}_i$ by three indices (ℓ_i, m_i, n_i) in three directions x, y and z.

Since there is the translation invariance in the xy plane, the in-plane Fourier transforms of the above equations are

$$\begin{aligned}
G_{i,j}(t,t') &= \frac{1}{\Delta}\int\int_{BZ} d\mathbf{k}_{xy}\frac{1}{2\pi}\int_{-\infty}^{+\infty} d\omega e^{-i\omega(t-t')} \\
&\times g_{n_i,n_j}(\omega,\mathbf{k}_{xy})\, e^{i\mathbf{k}_{xy}\cdot(\mathbf{R}_i-\mathbf{R}_j)}, \qquad (19)\\
F_{k,j}(t,t') &= \frac{1}{\Delta}\int\int_{BZ} d\mathbf{k}_{xy}\frac{1}{2\pi}\int_{-\infty}^{+\infty} d\omega e^{-i\omega(t-t')} \\
&\times f_{n_k,n_j}(\omega,\mathbf{k}_{xy})\, e^{i\mathbf{k}_{xy}\cdot(\mathbf{R}_k-\mathbf{R}_j)}, \qquad (20)
\end{aligned}$$

where ω is the SW frequency, $\mathbf{k}_{xy}$ the wave-vector parallel to xy planes and $\mathbf{R}_i$ the position of $\mathbf{S}_i$. n_i, n_j and n_k indicate respectively the z-component indices of the layers where the sites $\mathbf{R}_i$, $\mathbf{R}_j$ and $\mathbf{R}_k$ belong to. The integral over $\mathbf{k}_{xy}$ is performed in the first Brillouin zone (BZ) whose surface is Δ in the xy reciprocal plane. $n_i = 1$ denotes the surface layer, $n_i = 2$ the second layer etc.

Preprints (www.preprints.org) | NOT PEER-REVIEWED | Posted: 18 July 2022 doi:10.20944/preprints202207.0268.v1

In the 3D case, the Fourier transformation of Eqs. (17)-(18) in three directions yields two coupled equations which can be solved to obtain the SW dispersion relation in the absence of anisotropy:

$$\hbar\omega = \pm\sqrt{A^2 - B^2} \tag{21}$$

where

$$\begin{aligned} A &= J_1 \langle S^z \rangle [\cos\theta + 1] Z\gamma + 2ZJ_1 \langle S^z \rangle \cos\theta \\ &\quad + J_2 \langle S^z \rangle [\cos(2\theta) + 1] Z_c \cos(k_z a) \\ &\quad + 2Z_c J_2 \langle S^z \rangle \cos(2\theta) \\ B &= J_1 \langle S^z \rangle (\cos\theta - 1) Z\gamma \\ &\quad + J_2 \langle S^z \rangle [\cos(2\theta) - 1] Z_c \cos(k_z a) \end{aligned}$$

where $Z = 8$ (NN number), $Z_c = 2$ (NNN number on the c-axis), $\gamma = \cos(k_x a/2)\cos(k_y a/2)\cos(k_z a/2)$ (a: lattice constant). We see that $\hbar\omega$ is zero when $A = \pm B$, namely at $k_x = k_y = k_z = 0$ ($\gamma = 1$) and at $k_z = 2\theta$ along the helical axis. The case of ferromagnets (antiferromagnets) with NN interaction only is recovered by putting $\cos\theta = 1$ (-1) [2].

In the case of a thin film, the in-plane Fourier transformation yields the following matrix equation

$$\mathbf{M}(\omega)\,\mathbf{h} = \mathbf{u}, \tag{22}$$

where $\mathbf{h}$ and $\mathbf{u}$ are the column matrices which are defined as follows

$$\mathbf{h} = \begin{pmatrix} g_{1,n'} \\ f_{1,n'} \\ \vdots \\ g_{n,n'} \\ f_{n,n'} \\ \vdots \\ g_{N_z,n'} \\ f_{N_z,n'} \end{pmatrix}, \mathbf{u} = \begin{pmatrix} 2\langle S_1^z \rangle \delta_{1,n'} \\ 0 \\ \vdots \\ 2\left\langle S_{N_z}^z \right\rangle \delta_{N_z,n'} \\ 0 \end{pmatrix}, \tag{23}$$

We take $\hbar = 1$ hereafter. Note that $\mathbf{M}(\omega)$ is a square matrix of dimension $(2N_z \times 2N_z)$, given by Eq. (24) where

$$\begin{aligned} A_n &= -8J_1(1+d)\Big[\langle S_{n+1}^z \rangle \cos\theta_{n,n+1} \\ &\quad + \langle S_{n-1}^z \rangle \cos\theta_{n,n-1}\Big] \\ &- 2J_2\Big[\langle S_{n+2}^z \rangle \cos\theta_{n,n+2} \\ &\quad + \langle S_{n-2}^z \rangle \cos\theta_{n,n-2}\Big] \end{aligned}$$

where $n = 1, 2, ..., N_z$, $d = I_1/J_1$, and

$$\begin{aligned} B_n^{\pm} &= 4J_1 \langle S_n^z \rangle (\cos\theta_{n,n\pm1} + 1)\gamma \\ C_n^{\pm} &= 4J_1 \langle S_n^z \rangle (\cos\theta_{n,n\pm1} - 1)\gamma \\ E_n^{\pm} &= J_2 \langle S_n^z \rangle (\cos\theta_{n,n\pm2} - 1) \\ D_n^{\pm} &= J_2 \langle S_n^z \rangle (\cos\theta_{n,n\pm2} + 1) \end{aligned}$$

Preprints (www.preprints.org) | NOT PEER-REVIEWED | Posted: 18 July 2022 doi:10.20944/preprints202207.0268.v1

$$
\mathbf{M}(\omega) = \begin{pmatrix}
\omega + A_1 & 0 & B_1^+ & C_1^+ & D_1^+ & E_1^+ & 0 & 0 & 0 & 0 & 0 \\
0 & \omega - A_1 & -C_1^+ & -B_1^+ & -E_1^+ & -D_1^+ & 0 & 0 & 0 & 0 & 0 \\
\cdots & \cdots & \cdots & \cdots & \cdots & \cdots & \cdots & \cdots & \cdots & \cdots & \cdots \\
\cdots & \cdots & D_n^- & B_n^- & C_n^- & \omega + A_n & 0 & B_n^+ & C_n^+ & D_n^+ & E_n^+ \\
\cdots & \cdots & -E_n^- & -C_n^- & -B_n^- & 0 & \omega - A_n & -C_n^+ & -B_n^+ & -E_n^+ & -D_n^+ \\
\cdots & \cdots & \cdots & \cdots & \cdots & \cdots & \cdots & \cdots & \cdots & \cdots & \cdots \\
0 & 0 & 0 & 0 & 0 & 0 & D_{N_z}^- & E_{N_z}^- & B_{N_z}^- & C_{N_z}^- & \omega + A_{N_z} \\
0 & 0 & 0 & 0 & 0 & 0 & -E_{N_z}^- & -D_{N_z}^- & -C_{N_z}^- & -B_{N_z}^- & 0 \\
0 & 0 & 0 & 0 & 0 & 0 & 0 & 0 & 0 & 0 & \omega - A_{N_z}
\end{pmatrix}
\tag{24}
$$

Preprints (www.preprints.org) | NOT PEER-REVIEWED | Posted: 18 July 2022 doi:10.20944/preprints202207.0268.v1

where $\theta_{n,n\pm1}$ is the angle between a spin in the layer n and its NN spins in layers $n \pm 1$ etc. and $\gamma = \cos\left(\frac{k_x a}{2}\right)\cos\left(\frac{k_y a}{2}\right)$.

Solving $\det|\mathbf{M}| = 0$, we obtain the SW spectrum ω of the film for each value (k_x, k_y). There are $2N_z$ eigen-values of ω corresponding to two opposite spin precessions as in antiferromagnets (the dimension of $\det|\mathbf{M}|$ is $2N_z \times 2N_z$). Note that the above equation depends on the values of $< S_n^z >$ $(n = 1, ..., N_z)$. Even at temperature $T = 0$, these z-components are not equal to $1/2$ because we are dealing with a non-collinear system where fluctuations at $T = 0$ give rise to the so-called zero-point spin contraction [31]. In addition, because of the film surfaces, the spin contractions are not homogeneous as seen below. Therefore, the solution of $\det|\mathbf{M}| = 0$ should be obtained by iteration.

The solution for $g_{n,n}$ can be calculated. The reader is referred to Ref. [29] for details. Next, using the spectral theorem [1] which relates $\langle S_n^z \rangle$ to the spin-spin correlation we obtain, after a somewhat lengthy algebra (see [29]):

$$\langle S_n^z \rangle = \frac{1}{2} - \frac{1}{\Delta}\int\int dk_x dk_y \sum_{i=1}^{2N_z} \frac{D_{2n-1}(\omega_i)}{e^{\beta\omega_i} - 1} \tag{25}$$

where $n = 1, ..., N_z$, and

$$D_{2n-1}\left(\omega_i\left(\mathbf{k}_{xy}\right)\right) = \frac{|\mathbf{M}|_{2n-1}\left(\omega_i\left(\mathbf{k}_{xy}\right)\right)}{\prod_{j\neq i}\left[\omega_j\left(\mathbf{k}_{xy}\right) - \omega_i\left(\mathbf{k}_{xy}\right)\right]}. \tag{26}$$

As $< S_n^z >$ depends on the magnetizations of the neighboring layers via $\omega_i (i = 1, ..., 2N_z)$, we should solve by iteration the equations (2) written for all layers, namely for $n = 1, ..., N_z$, to obtain the magnetizations of layers 1, 2, 3, ..., N_z at a given temperature T. Note that by symmetry, $< S_1^z >=< S_{N_z}^z >$, $< S_2^z >=< S_{N_z-1}^z >$, $< S_3^z >=< S_{N_z-2}^z >$, and so on. Thus, only $N_z/2$ self-consistent layer magnetizations are to be calculated. The value of the spin in the layer n at $T = 0$ is

$$\langle S_n^z \rangle (T = 0) = \frac{1}{2} + \frac{1}{\Delta}\int\int dk_x dk_y \sum_{i=1}^{N_z} D_{2n-1}(\omega_i\left(\mathbf{k}_{xy}\right)) \tag{27}$$

where the sum is done over only N_z negative values of ω_i (because for positive of ω_i , the Bose-Einstein factor is equal to 0 at $T = 0$).

The transition temperature T_c can be calculated in a self-consistent manner by iteration, letting all $< S_n^z >$ tend to zero, namely $\omega_i \to 0$.

We show in the following section, the numerical results using the above formulas.

3. Results for helimagnets obtained from the Green's function method

In the following we take the ferromagnetic interaction between NN $J_1 = 1$,. We consider the helimagnetic case where the NNN interaction J_2 is negative and $|J_2| > J_1$. The non-uniform GS spin configuration across the film has been determined above for each value of $p = J_2/J_1$. Using the values of $\theta_{n,n\pm1}$ and $\theta_{n,n\pm2}$ to calculate the matrix elements of $|\mathbf{M}|$, then solving $\det|\mathbf{M}| = 0$ we find the eigenvalues $\omega_i (i = 1, ..., 2N_z)$ for each $\mathbf{k}_{xy}$ with a input set of $\langle S_n^z \rangle (n = 1, ..., N_z)$ at a given T. Using Eq. (2) for $n = 1, ..., N_z$ we calculate the output $\langle S_n^z \rangle (n = 1, ..., N_z)$. Using this output set as input, we calculate again $\langle S_n^z \rangle (n = 1, ..., N_z)$ until the input and output are identical within a desired precision P. Numerically, we use a Brillouin zone of 100^2 wave-vector values, and we use the obtained values $\langle S_n^z \rangle$ at a given T as input for a neighboring T. At low T and up to $\sim \frac{4}{5}T_c$, only a few iterations suffice to get $P \leq 1\%$. Near T_c, several dozens of iteration are needed to get convergence. We show below our results.

Preprints (www.preprints.org) | NOT PEER-REVIEWED | Posted: 18 July 2022 doi:10.20944/preprints202207.0268.v1

3.1. Spectrum

We calculate the SW spectrum as described above for each a given J_2/J_1. The SW spectrum depends on the temperature via the temperature-dependence of layer magnetizations. Let us show in Fig. 4 the SW frequency ω versus $k_x = k_y$ in the case of an 8-layer film where $J_2/J_1 = -1.4$ at two temperatures $T = 0.1$ and $T = 1.02$ (in units of $J_1/k_B = 1$). Some remarks are in order:

(i) There are 8 positive and 8 negative modes corresponding two opposite spin precessions. Unlike ferromagnets, SW in antiferromagnets and non collinear spin structures have opposite spin precessions which describe the opposite circular motion of each sublattice spins [31]. The negative sign does not mean SW negative energy, but it indicates just the precession contrary to the trigonometric sense,
(ii) Note that there are two degenerate acoustic surface branches lying at low energy on each side. This degeneracy comes from the two symmetrical surfaces of the film. These surface modes propagate parallel to the film surface but are damped from the surface inward,
(iii) As T increases, layer magnetizations decrease (see below), reducing therefore the SW energy as seen in Fig. 4 (bottom),
(iv) If the spin magnitude $S \neq 1/2$, then the spectrum is shifted toward higher frequency since it is proportional to S,
(v) Surface SW spectrum (and bulk SW) can be experimentally observed by inelastic neutron scattering in ferromagnetic and antiferromagnetic films [32,33]. To our knowledge, such experiments have not been performed for helimagnets.

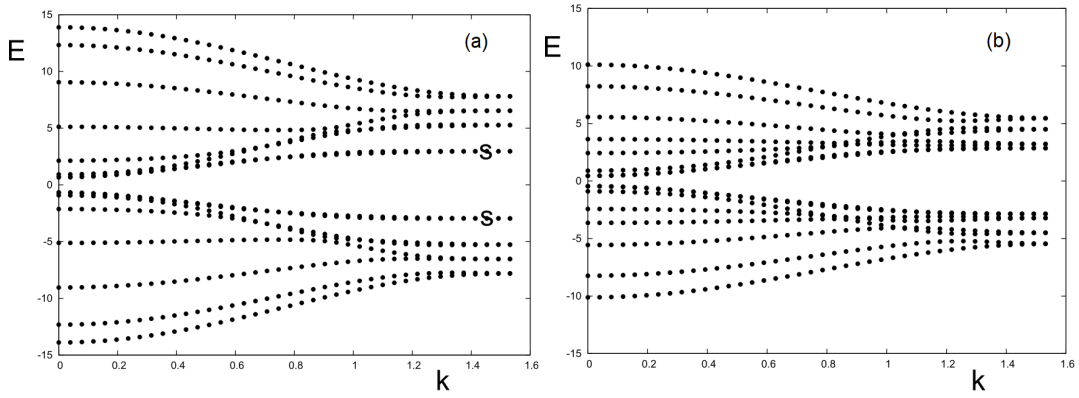

Figure 4. (a) Spectrum $E = \hbar\omega$ versus $k \equiv k_x = k_y$ for $J_2/J_1 = -1.4$ at $T = 0.1$ and (b) $T = 1.02$, for $N_z = 8$ and $d = 0.1$. The surface branches are indicated by s.

3.2. Spin contraction at $T = 0$ and transition temperature

In antiferromagnets, quantum fluctuations give rise to a contraction of the spin length at zero temperature [31]. We will see here that a spin under a stronger antiferromagnetic interaction has a stronger zero-point spin contraction. The spins near the surface serve for such a test. In the case of the film considered above, spins in the first and in the second layers have only one antiferromagnetic NNN while interior spins have two NNN, so the contraction at a given J_2/J_1 is expected to be stronger for interior spins. This is verified with the results shown in Fig. 5. When $|J_2|/J_1$ increases, i.e. the antiferromagnetic interaction becomes stronger, we observe stronger contractions. Note that the contraction tends to zero when the spin configuration becomes ferromagnetic, namely J_2 tends to -1.

3.3. Layer magnetizations

We show now two examples of the magnetization, layer by layer, from the film surface in Figs. 6 and 7, for the case where $J_2/J_1 = -1.4$ and -2 in a $N_z = 8$ film. Let us comment on the case $J_2/J_1 = -1.4$:

Preprints (www.preprints.org) | NOT PEER-REVIEWED | Posted: 18 July 2022 doi:10.20944/preprints202207.0268.v1

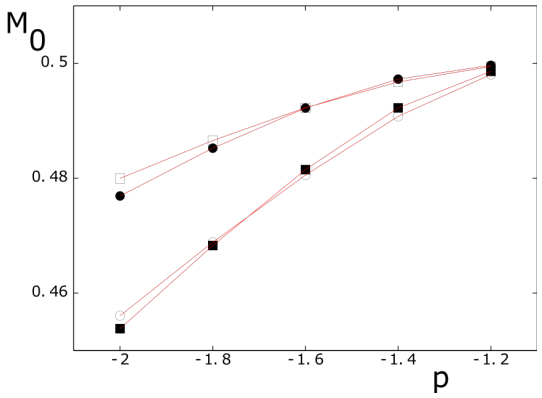

Figure 5. (Spin lengths of the first four layers at $T = 0$ for several values of $p = J_2/J_1$ with $d = 0.1$, $N_z = 8$. As seen, all are contracted to values smaller than the spin magnitude $1/2$. Black circles, void circles, black squares and void squares are for first, second, third and fourth layers, respectively.

(i) the shown result is obtained with a convergence of 1%. For temperatures closer to the transition temperature T_c, we have to lower the precision to a few percents which reduces the clarity because of their close values (not shown).

(ii) the surface magnetization, which has a large value at $T = 0$ as seen in Fig. 5, crosses the interior layer magnetizations at $T \simeq 0.42$ to become much smaller than interior magnetizations at higher temperatures. This crossover phenomenon is due to the competition between quantum fluctuations, which dominate low-T behavior, and the low-lying surface SW modes which strongly diminish the surface magnetization at higher T. Note that the second-layer magnetization makes also a crossover at $T \simeq 1.3$. Similar crossovers have been observed in quantum antiferromagnetic films [34] and quantum superlattices [35].

Similar remarks can be also made for the case $J_2/J_1 = -2$.

Note that though the layer magnetizations are different at low temperatures, they will tend to zero at a unique transition temperature as seen below. The reason is that as long as an interior layer magnetization is not zero, it will act on the surface spins as an external field, preventing them to become zero.

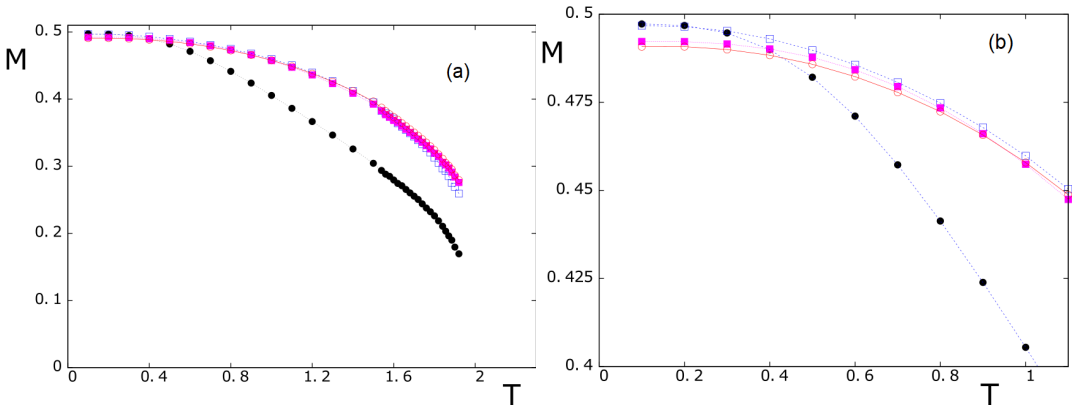

Figure 6. (a) Layer magnetizations as functions of T for $J_2/J_1 = -1.4$ with $d = 0.1$, $N_z = 8$, (b) Zoom of the region at low T to show crossover. Black circles, blue void squares, magenta squares and red void circles are for first, second, third and fourth layers, respectively. See text.

Note that the results shown above have been calculated with an in-plane anisotropy interaction $d = 0.1$. The use of stronger d will enhance all the layer magnetizations and increase T_c.

To close this section on SW in helimagnetic bct thin films, we mention that a similar investigation has been carried out in the case of helimagnetic films of simple cubic lattice where the surface spin reconstruction and the surface SW have been shown. [36] We have also studied the frustrated bct

Preprints (www.preprints.org) | NOT PEER-REVIEWED | Posted: 18 July 2022 doi:10.20944/preprints202207.0268.v1

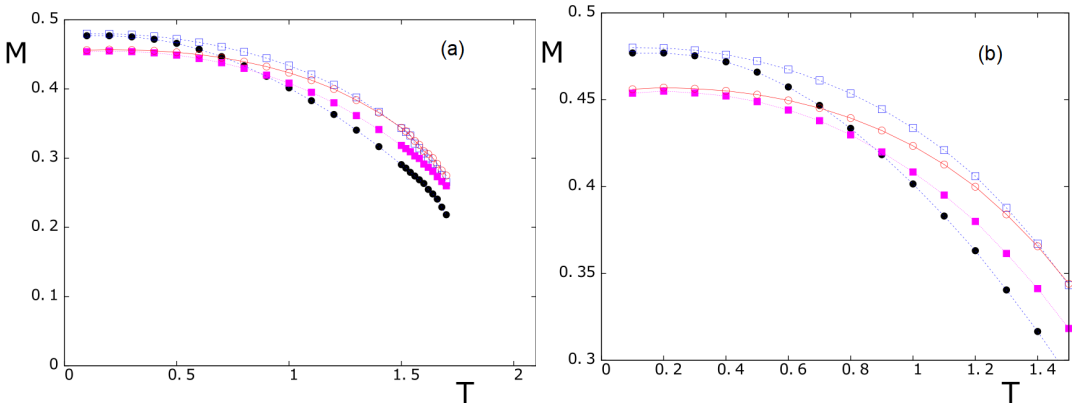

Figure 7. (a) Layer magnetizations as functions of T for $J_2/J_1 = -2$ with $d = 0.1$, $N_z = 8$, (b) Zoom of the region at low T to show crossover. Black circles, blue void squares, magenta squares and red void circles are for first, second, third and fourth layers, respectively. See text.

Heisenberg helimagnet in which the SW spectrum of the non-collinear spin configuration has been calculated.[37]

4. Dzyaloshinskii-Moriya interaction in thin films: model and ground state

We consider a thin film of simple cubic (SC) lattice of N layers stacked in the y direction perpendicular to the film surface. The results for this system have been published in Ref. [38]. Hereafter, we review some of these important results. The Hamiltonian is given by

$$\mathcal{H} = \mathcal{H}_e + \mathcal{H}_{DM} \quad (28)$$

$$\mathcal{H}_e = -\sum_{\langle i,j \rangle} J_{i,j} \mathbf{S}_i \cdot \mathbf{S}_j \quad (29)$$

$$\mathcal{H}_{DM} = \sum_{\langle i,j \rangle} \mathbf{D}_{i,j} \cdot \mathbf{S}_i \times \mathbf{S}_j \quad (30)$$

where $J_{i,j}$ and $\mathbf{D}_{i,j}$ are the exchange and DM interactions, respectively, between two Heisenberg spins $\mathbf{S}_i$ and $\mathbf{S}_j$ of magnitude $S = 1/2$ occupying the lattice sites i and j.

As in the previous section we consider the case where the in-plane and inter-plane exchange interactions between NN are both ferromagnetic and denoted by J_1 and J_2, respectively. The DM interaction is supposed to be between NN in the plane with a constant D. Due to the competition between the exchange J term which favors the collinear configuration, and the DM term which favors the perpendicular one, we expect that the spin $\mathbf{S}_i$ makes an angle $\theta_{i,j}$ with its neighbor $\mathbf{S}_j$. Therefore, the quantization axis of $\mathbf{S}_i$ is not the same as that of $\mathbf{S}_j$. Let us use the transformation to the local coordinates, Eqs. (4)-(9). We choose the vector $\mathbf{D}_{i,j}$ perpendicular to the xz plane, namely

$$\mathbf{D}_{i,j} = D e_{i,j} \hat{\eta}_i \quad (31)$$

where $e_{i,j}$ =+1 (-1) if $j > i$ ($j < i$) for NN on the $\hat{\xi}_i$ or $\hat{\zeta}_i$ axis. Note that $e_{j,i} = -e_{i,j}$.

To determine the GS, the easiest way is to use the steepest descent method: we calculate the local field acting on each spin from its neighbors and we align the spin in its local-field direction to minimize its energy. Repeating this for all spins and iterating many times until the convergence is reached with a desired precision (usually at the 6-th digit, namely at $\simeq 10^{-6}$ per cents), we obtain the lowest energy state of the system (see Ref. [39]). Note that we have used several thousands of different initial conditions to check the convergence to a single GS for each set of parameters. Choosing $\mathbf{D}_{i,j}$

Preprints (www.preprints.org) | NOT PEER-REVIEWED | Posted: 18 July 2022 doi:10.20944/preprints202207.0268.v1

lying perpendicular to the spin plane (i. e. xz plane) as indicated in Eq. (31), we determine the GS as a function of D. An example is shown in Fig. 8 for $D = -0.5$ with $J_1 = J_2 = 1$.

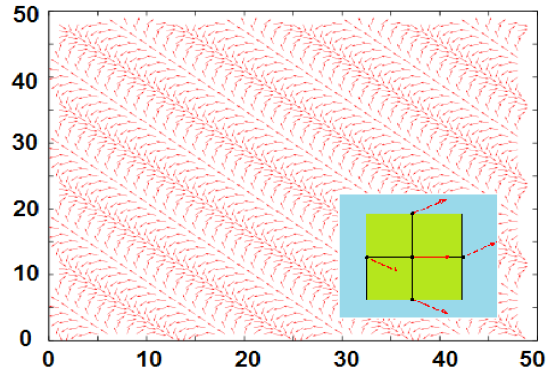

Figure 8. The ground state is a planar configuration on the xz plane. The figure shows the case where $\theta = \pi/6$ ($D = -0.577$), $J_1 = J_\perp = 1$ using the steepest descent method. The inset shows a zoom around a spin with its nearest neighbors.

We see that each spin has the same angle with its four NN in the plane (angle between NN in adjacent planes is zero). Let us show the relation between θ and J_1: the energy of the spin $\mathbf{S}_i$ is written as

$$E_i = -4J_1S^2\cos\theta - 2J_2S^2 + 4DS^2\sin\theta \tag{32}$$

where $\theta = |\theta_{i,j}|$ and care has been taken on the signs of $\sin\theta_{i,j}$ and $e_{i,j}$ when counting NN, namely two opposite NN have opposite signs. The minimization of E_i yields

$$\frac{dE_i}{d\theta} = 0 \;\Rightarrow\; -\frac{D}{J_1} = \tan\theta \;\Rightarrow\; \theta = \arctan(-\frac{D}{J_1}) \tag{33}$$

The value of θ for a given $\frac{D}{J_1}$ is precisely what obtained by the steepest descent method.

In the present model, the DM interaction is supposed in the plane, so in the GS the angle between in-plane NN is not zero. We show in Fig. 8 the relative orientation of the two NN spins in the plane.

The DM term of Eq. (30) can be rewritten as

$$\begin{aligned}\mathbf{S}_i \times \mathbf{S}_j &= (-S_i^zS_j^y - S_i^yS_j^x\sin\theta_{i,j} + S_i^yS_j^z\cos\theta_{i,j})\hat{\xi}_i \\ &+(S_i^xS_j^x\sin\theta_{i,j} + S_i^zS_j^z\sin\theta_{i,j})\hat{\eta}_i \\ &+(S_i^xS_j^y - S_i^yS_j^z\sin\theta_{i,j} - S_i^yS_j^x\cos\theta_{i,j})\hat{\zeta}_i\end{aligned} \tag{34}$$

Using Eq. (31), we have

$$\begin{aligned}\mathcal{H}_{DM} &= \sum_{\langle i,j\rangle}\mathbf{D}_{i,j}\cdot\mathbf{S}_i\times\mathbf{S}_j \\ &= D\sum_{\langle i,j\rangle}(S_i^xS_j^xe_{i,j}\sin\theta_{i,j} + S_i^zS_j^ze_{i,j}\sin\theta_{i,j}) \\ &= \frac{D}{4}\sum_{\langle i,j\rangle}[(S_i^+ + S_i^-)(S_j^+ + S_j^-)e_{i,j}\sin\theta_{i,j} \\ &\quad +4S_i^zS_j^ze_{i,j}\sin\theta_{i,j}]\end{aligned} \tag{35}$$

Preprints (www.preprints.org) | NOT PEER-REVIEWED | Posted: 18 July 2022 doi:10.20944/preprints202207.0268.v1

where we have replaced $S^x = (S^+ + S^-)/2$. Note that $e_{i,j} \sin\theta_{i,j}$ is always positive since for a NN on the positive axis direction, $e_{i,j} = 1$ and $\sin\theta_{i,j} = \sin\theta$ where θ is positively defined, while for a NN on the negative axis direction, $e_{i,j} = -1$ and $\sin\theta_{i,j} = \sin(-\theta) = -\sin\theta$.

4.1. Self-consistent Green's function method for the Dzyaloshinskii-Moriya system

Expressing the Hamiltonian in the local coordinates using Eqs. (4)-(9), we obtain

$$\begin{aligned}
\mathcal{H} &= -\sum_{<i,j>} J_{i,j} \Bigg\{ \frac{1}{4}\left(\cos\theta_{i,j} - 1\right)\left(S_i^+ S_j^+ + S_i^- S_j^-\right) \\
&+ \frac{1}{4}\left(\cos\theta_{i,j} + 1\right)\left(S_i^+ S_j^- + S_i^- S_j^+\right) \\
&+ \frac{1}{2}\sin\theta_{i,j}\left(S_i^+ + S_i^-\right) S_j^z - \frac{1}{2}\sin\theta_{i,j} S_i^z \left(S_j^+ + S_j^-\right) \\
&+ \cos\theta_{i,j} S_i^z S_j^z \Bigg\} \\
&+ \frac{D}{4}\sum_{\langle i,j\rangle} [(S_i^+ + S_i^-)(S_j^+ + S_j^-) e_{i,j} \sin\theta_{i,j} \\
&\quad + 4 S_i^z S_j^z e_{i,j} \sin\theta_{i,j}]
\end{aligned} \tag{36}$$

As said in the previous section, the spins lie in the xz planes, each on its quantization local z axis (Fig. 3).

Note that unlike the sinus term of the DM Hamiltonian, Eq. (35), the sinus terms of $\mathcal{H}_e$, the 3rd line of Eq. (36), are zero when summed up on opposite NN (no $e_{i,j}$ to compensate). The 3rd line disappears therefore in the following.

At this stage it is very important to note that the standard commutation relations between spin operators S^z and $S^\pm$ are defined with z as the spin quantization axis. In non-collinear spin configurations, calculations of SW spectrum using commutation relations without paying attention to this are wrong.

It is known that in two dimensions (2D) there is no long-range order at finite temperature (T) for isotropic spin models with short-range interaction [40]. Thin films have small thickness, therefore to stabilize the ordering at finite T it is useful to add an anisotropic interaction. We use the following anisotropy between $\mathbf{S}_i$ and $\mathbf{S}_j$ which stabilizes the angle determined above between their local quantization axes S_i^z and S_j^z:

$$\mathcal{H}_a = -\sum_{<i,j>} I_{i,j} S_i^z S_j^z \cos\theta_{i,j} \tag{37}$$

where $I_{i,j} (> 0)$ is supposed to be positive, small compared to J_1, and limited to NN. Hereafter we take $I_{i,j} = I_1$ for NN pair in the xz plane, for simplicity. As it turns out, this anisotropy does not only stabilize the ordering at finite T as discussed but, as seen below, it does also stabilize the SW spectrum when D becomes large. The total Hamiltonian is finally given by

$$\mathcal{H} = \mathcal{H}_e + \mathcal{H}_{DM} + \mathcal{H}_a \tag{38}$$

We define the two double-time GF's in the real space as in Eqs. (11)-(12) and we use the same method as in that part. For the DM term, the commutation relations $[\mathcal{H}, S_i^\pm]$ give rise to the following term:

$$D\sum_l \sin\theta [\mp S_i^z (S_l^+ + S_l^-) + \pm 2 S_i^\pm S_l^z] \tag{39}$$

Preprints (www.preprints.org) | NOT PEER-REVIEWED | Posted: 18 July 2022 doi:10.20944/preprints202207.0268.v1

which gives rise to the following type of GF's:

$$<< S_i^z S_l^{\pm}; S_j^- >> \simeq < S_i^z > << S_l^{\pm}; S_j^- >> \tag{40}$$

Note that we have replaced $e_{i,j} \sin\theta_{i,j}$ by $\sin\theta$ where θ is positive. The above equation is thus related to G and F functions. The Tyablikov decoupling scheme citeTyablikov neglects higher-order functions.

As in section 2, the in-plane Fourier transforms $g_{n,n'}$ and $f_{n,n'}$ of the G and F lead to the following matrix equation

$$\mathbf{M}(E)\,\mathbf{h} = \mathbf{u}, \tag{41}$$

where $\mathbf{M}(E)$ is given by Eq. (42) below where $E = \hbar\omega$ is the SW energy and the matrix elements are given by

$$\begin{aligned} A_n &= -J_1[8 < S_n^z > \cos\theta(1+d_n) \\ &\quad -4 < S_n^z > \gamma(\cos\theta + 1)] \\ &\quad -2J_2(< S_{n-1}^z > + < S_{n+1}^z >) \\ &\quad -8D\sin\theta < S_n^z > \gamma \\ &\quad +8D\sin\theta < S_n^z > \qquad (43) \\ B_n &= 4J_1 < S_n^z > \gamma(\cos\theta - 1) \\ &\quad -8D\sin\theta < S_n^z > \gamma \qquad (44) \\ C_n &= 2J_2 < S_n^z > \qquad (45) \end{aligned}$$

where $n = 1, 2, ..., N$, $d_n = I_1/J_1$, $\gamma = (\cos k_x a + \cos k_z a)/2$, k_x and k_z denote the wave-vector components in the xz planes, a the lattice constant. Note that (i) if $n = 1$ (surface layer) then there are no $n-1$ terms in the matrix coefficients, (ii) if $n = N$ then there are no $n+1$ terms. Besides, we have distinguished the in-plane NN interaction J_1 from the inter-plane NN one $J_\perp$.

In the case of a thin film, the SW eigenvalues at a given wave vector $\vec{k} = (k_x, kz)$ are calculated by diagonalizing the matrix (42).

The layer magnetization of the layer n at finite T is calculated as in the helimagnetic case shown in the previous section. The value of the spin in the layer n at $T = 0$ is also outlined there. The transition temperature T_c can be also calculated by the same method. Let us show in the following the results.

4.2. Two and three dimensions: spin-wave spectrum and magnetization

Consider just one single xz plane. The above matrix is reduced to two coupled equations

$$\begin{aligned} (E + A_n)g_{n,n'} + B_n f_{n,n'} &= 2 < S_n^z > \delta(n, n') \\ -B_n g_{n,n'} + (E - A_n)f_{n,n'} &= 0 \end{aligned} \tag{46}$$

where A_n is given by (43) but without $J_\perp$ term for the 2D case considered here. Coefficients B_n and C_n are given by (44) and (45) with $C_n = 0$. The poles of the GF are the eigenvalues of the SW spectrum which are given by the secular equation

$$\begin{aligned} &(E + A_n)(E - A_n) + B_n^2 = 0 \\ &[E + A_n][E - A_n] + B_n^2 = 0 \\ &E^2 - A_n^2 + B_n^2 = 0 \\ &E = \pm\sqrt{(A_n + B_n)(A_n - B_n)} \end{aligned} \tag{47}$$

Several remarks are in order:

Preprints (www.preprints.org) | NOT PEER-REVIEWED | Posted: 18 July 2022 doi:10.20944/preprints202207.0268.v1

$$
\begin{pmatrix}
E+A_1 & B_1 & C_1 & 0 & 0 & 0 & 0 & 0 & 0 \\
-B_1 & E-A_1 & 0 & -C_1 & 0 & 0 & 0 & 0 & 0 \\
\cdots & \cdots & \cdots & \cdots & \cdots & \cdots & \cdots & \cdots & \cdots \\
\cdots & 0 & C_n & 0 & E+A_n & B_n & C_n & 0 & 0 \\
\cdots & 0 & 0 & -C_n & -B_n & E-A_n & 0 & -C_n & 0 \\
\cdots & \cdots & \cdots & \cdots & \cdots & \cdots & \cdots & \cdots & \cdots \\
0 & 0 & 0 & 0 & 0 & C_N & 0 & E+A_N & B_N \\
0 & 0 & 0 & 0 & 0 & 0 & -C_N & -B_N & E-A_N
\end{pmatrix}
\tag{42}
$$

Preprints (www.preprints.org) | NOT PEER-REVIEWED | Posted: 18 July 2022 doi:10.20944/preprints202207.0268.v1

(i) if $\theta = 0$, we have $B_n = 0$ and the last three terms of A_n are zero. We recover then the ferromagnetic SW dispersion relation

$$E = 2ZJ_1 < S_n^z > (1 - \gamma) \tag{48}$$

where $Z = 4$ is the coordination number of the square lattice (taking $d_n = 0$),

(ii) if $\theta = \pi$, we have $A_n = 8J_1 < S_n^z >$, $B_n = -8J_1 < S_n^z > \gamma$. We recover then the antiferromagnetic SW dispersion relation

$$E = 2ZJ_1 < S_n^z > \sqrt{1 - \gamma^2} \tag{49}$$

(iii) in the presence of a DM interaction, we have $0 < \cos\theta < 1$ ($0 < \theta < \pi/2$). If $d_n = 0$, the quantity in the square root of Eq. (47) becomes negative at $\gamma = 1$ when θ is not zero. The SW spectrum is not stable at the long-wavelength limit because the energy is not real. The anisotropy d_n can remove this instability if it is larger than a threshold value d_c. We solve the equation $(A_n + B_n)(A_n - B_n) = 0$ to find d_c. In Fig. 9 we show d_c as a function of θ (in radian). As seen, d_c increases from zero with increasing θ.

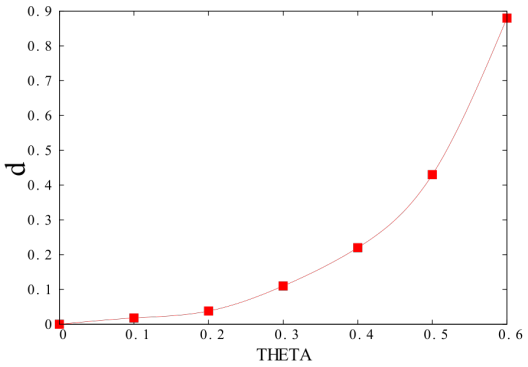

Figure 9. Value d_c at which $E = 0$ at $\gamma = 1$ ($\vec{k} = 0$) vs θ (in radian). Above this value, E is real. See text for comments.

As said earlier, the necessity to include an anisotropy has a double purpose: it permits SW excitations and stabilizes a long-range ordering at finite T in 2D systems.

Figure 10 shows the SW spectrum calculated from Eq. (47) for $\theta = 0.2$ and 0.6 (radian). The spectrum is symmetric for positive and negative wave vectors and for left and right precessions. Note that for small θ (i. e. small D) E is proportional to k^2 at low k (cf. 10a), as in ferromagnets. However, as θ increases, we observe that E becomes linear in k as seen in Fig. 10b. This is similar to antiferromagnets. The change of behavior is progressive with increasing θ, we do not observe a sudden transition from k^2 to k behavior. This feature is also observed in three dimensions (3D) and in thin films as seen below.

As said earlier, thanks to the existence of the anisotropy d, we can observe a long-range ordering at finite T in 2D. We show in Fig. 11 the magnetization M ($\equiv < S^z >$) calculated by Eq. (83) for one layer using in each case the limit value d_c. It is interesting to observe that M depends strongly on θ: at high T the larger θ the stronger M. However, at $T = 0$ the spin length is smaller for larger θ due to the so-called spin contraction [31] calculated by Eq. (27). As a consequence there is a cross-over des magnetizations at low T as shown in Fig. 11b. The spin length at $T = 0$ is shown in Fig. 12 for several θ.

Preprints (www.preprints.org) | NOT PEER-REVIEWED | Posted: 18 July 2022 doi:10.20944/preprints202207.0268.v1

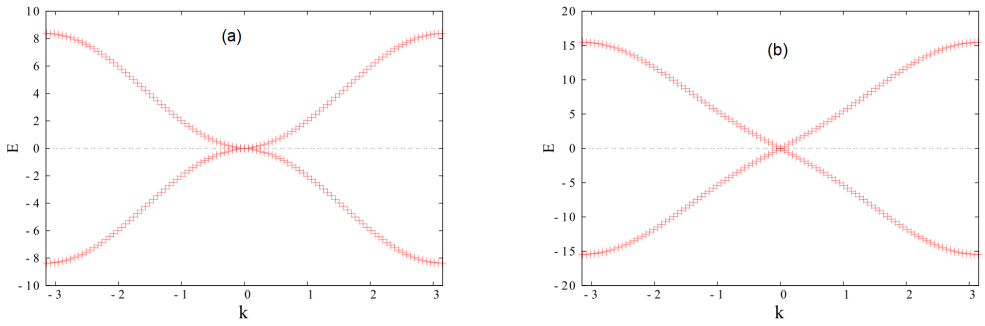

Figure 10. Spin-wave spectrum $E(k)$ versus $k \equiv k_x = k_z$ for (a) $\theta = 0.2$ and (b) $\theta = 0.6$ in two dimensions. Positive and negative branches correspond to right and left precessions. See text for comments.

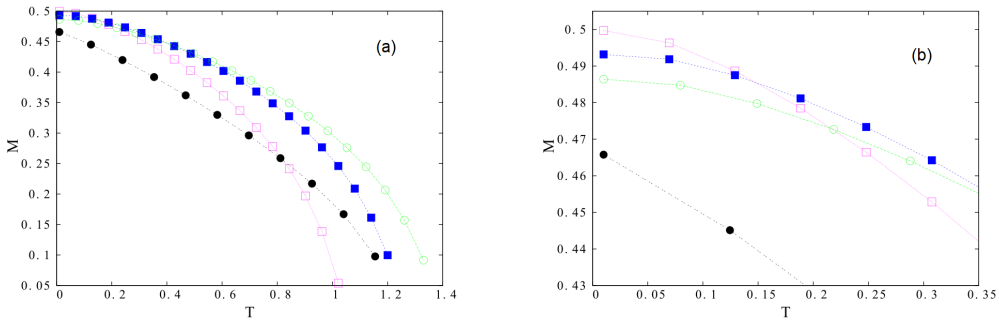

Figure 11. (a) Layer magnetizations M versus temperature T for a monolayer (2D) $\theta = 0.1$ (radian), $\theta = 0.3$, $\theta = 0.4$, $\theta = 0.6$ (void magenta squares, blue filled squares, green void circles and filled black circles, respectively), (b) Zoom to highlight the cross-over of magnetizations at low T. See text for comments.

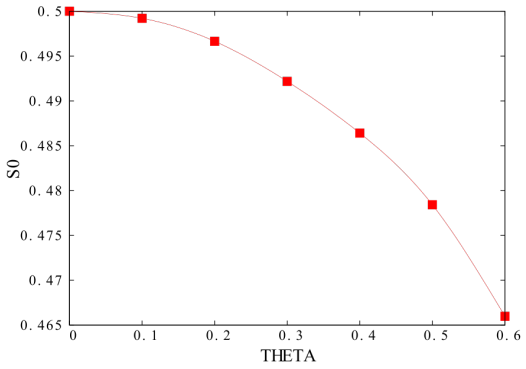

Figure 12. Spin length at temperature $T = 0$ for a monolayer (2D) versus θ (radian).

Let us study the 3D case. The crystal is periodic in three direction. We can use the Fourier transformation in the y direction, namely $g_{n\pm1} = g_n e^{\pm ik_y a}$ and $f_{n\pm1} = f_n e^{\pm ik_y a}$. The matrix (23) is reduced to two coupled equations of g and f functions, omitting index n,

$$\begin{aligned} (E + A')g + Bf &= 2 < S^z > \\ -Bg + (E - A')f &= 0 \end{aligned} \tag{50}$$

Preprints (www.preprints.org) | NOT PEER-REVIEWED | Posted: 18 July 2022 doi:10.20944/preprints202207.0268.v1

where

$$\begin{aligned} A' &= -J_1[8 < S^z > \cos\theta(1+d) \\ &\quad -4 < S^z > \gamma(\cos\theta + 1)] \\ &\quad -4J_2 < S^z > \\ &\quad +4J_2 < S^z > \cos(k_y a) \\ &\quad -8D\sin\theta < S^z > \gamma \\ &\quad +8D\sin\theta < S^z > \qquad (51) \\ B &= 4J_1 < S^z > \gamma(\cos\theta - 1) \\ &\quad -8D\sin\theta < S^z > \gamma \qquad (52) \end{aligned}$$

The spectrum is given by

$$E = \pm\sqrt{(A'+B)(A'-B)} \qquad (53)$$

If $\cos\theta = 1$ (ferromagnetic), one has $B = 0$. By regrouping the Fourier transforms in three directions, one obtains the 3D ferromagnetic dispersion relation $E = 2Z < S^z > (1-\gamma^2)$ where $\gamma = [\cos(k_x a) + \cos(k_y a) + \cos(k_z a)]/3$ and $Z = 6$, coordination number of the simple cubic lattice. Unlike the 2D case where the angle is inside the plane so that the antiferromagnetic case can be recovered by setting $\cos\theta = -1$ as seen above, one cannot use the above formula to find the antiferromagnetic case because in the 3D formulation it was supposed a ferromagnetic coupling between planes, namely there is no angle between adjacent planes in the formulation.

The same consideration as in the 2D case treated above shows that the threshold value d_c is the same for a given θ. This is rather obvious because the DM interaction operates in the plane making an angle θ between spins in the plane, therefore its effects act on SW in each plane, not in the y direction perpendicular to the "DM planes". Using Eq. (53), we have calculated the 3D spectrum. This is shown in Fig. 13 for a small and a large value of θ. As in the 2D case, we observe $E \propto k$ when $k \to 0$ for large θ. As mentioned, main properties of the system are dominated by the in-plane DM behavior.

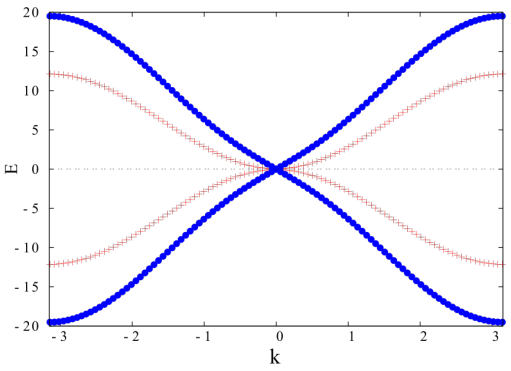

Figure 13. Spin-wave spectrum $E(k)$ versus $k \equiv k_x = k_z$ for $\theta = 0.1$ (red crosses) and $\theta = 0.6$ (blue circles) in three dimensions. Note the linear-k behavior at low k for the large value of θ. See text for comments.

Figure 14 displays the magnetization M versus T for several values of θ. As in the 2D case, when θ is not zero, the spins have a contraction at $T = 0$: the stronger θ the stronger contraction. This generates a magnetization cross-over at low T shown in Fig. 14b. The spin length at $T = 0$ versus θ is shown in Fig. 14c. Note that the spin contraction in 3D is smaller than in 2D. This is expected since quantum fluctuations are stronger at lower dimensions.

Preprints (www.preprints.org) | NOT PEER-REVIEWED | Posted: 18 July 2022 doi:10.20944/preprints202207.0268.v1

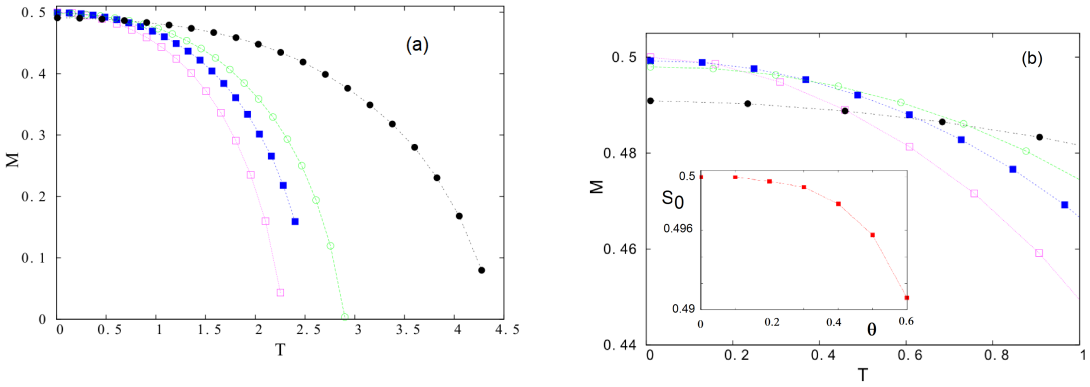

Figure 14. (a) Magnetization M versus temperature T for a 3D crystal $\theta = 0.1$ (radian), $\theta = 0.3$, $\theta = 0.4$, $\theta = 0.6$ (void magenta squares, blue filled squares, green void circles and filled black circles, respectively), (b) Zoom to show the cross-over of magnetizations at low T for different θ, inset shows S_0 versus θ. See text for comments.

4.3. The case of a thin film: spin-wave spectrum, layer magnetizations

Depending on θ, we have to use a value for d_n larger or equal to d_c given in Fig. 9 to avoid imaginary SW energies at long wave-length. There are $2N$ energy values half of them are positive and the other half negative: E_i $(i = 1, ..., 2N)$. Note that for thin films with more than one layer, the value of d_c calculated for the 2D case remains valid.

We show in Fig. 15 the SW spectrum for a film of 8 layers with $J_1 = J_\perp = 1$ for weak and strong D (small and large θ). As in the 2D and 2D cases, for strong D, E is proportional to k (cf. Fig. 15b). It is noted that this behavior concerns only the first mode. the upper modes remain in k^2.

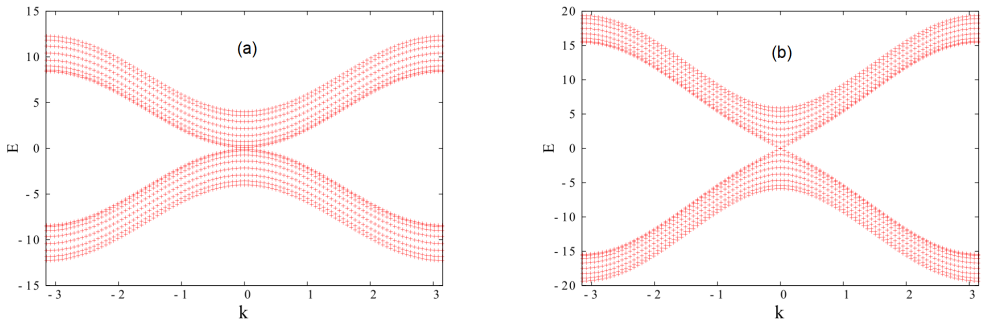

Figure 15. Spin-wave spectrum $E(k)$ versus $k \equiv k_x = k_z$ for a thin film of 8 layers: (a) $\theta = 0.2$ (in radian) (b) $\theta = 0.6$, using d_c for each case. Positive and negative branches correspond to right and left precessions. Note the linear-k behavior at low k. See text for comments.

Figure 16 shows the layer magnetizations of the first four layers in a 8-layer film (the other half is symmetric) for several values of θ. In each case, we see that the surface layer magnetization is smallest. This is the effect of the lack of neighbors for surface spins [2].

When θ becomes large, the contraction of the spin length at $T = 0$ is stronger. This is shown in Fig. 16c.

The effects of the surface exchange and the film thickness have been shown in Ref. [38].

To close this section, let us mention our work [41] on the DM interaction in magneto-ferroelectric superlattices where the SW in the magnetic layer have been calculated. We have also studied the stability of skyrmions at finite T in that work and in Refs. [42,43].

Preprints (www.preprints.org) | NOT PEER-REVIEWED | Posted: 18 July 2022 doi:10.20944/preprints202207.0268.v1

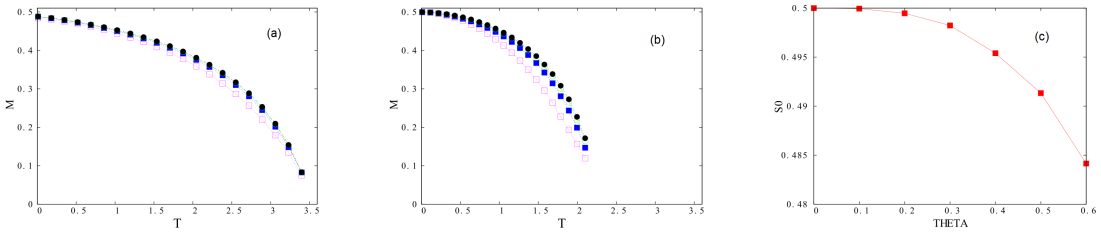

Figure 16. Layer magnetizations M versus temperature T for a thin film of 8 layers: (a) $\theta = 0.6$ (radian), (b) $\theta = 0.2$, (c) S_0 versus θ.

5. Effect of Dzyaloshinskii-Moriya interaction in a frustrated antiferromagnetic triangular lattice

The results of this section are not yet published [44]. We will not present this model in details. We show the Hamiltonian, the GS and the SW spectrum.

5.1. Model and Ground State

We consider a triangular lattice where the lattice site i is occupied by a Heisenberg spin $\mathbf{S}_i$ of magnitude 1. We suppose that $\mathbf{D}_{i,j}$ is a vector perpendicular to the xy plane and is given by [45,46]

$$\mathbf{D}_{i,j} \propto \mathbf{r}_{iO} \times \mathbf{r}_{Oj} \propto \mathbf{r}_{ij} \times \mathbf{R} \tag{54}$$

where $\mathbf{r}_{iO} = \mathbf{r}_O - \mathbf{r}_i$ and $\mathbf{r}_{Oj} = \mathbf{r}_j - \mathbf{r}_O$, $\mathbf{r}_{ij} = \mathbf{r}_j - \mathbf{r}_i$. $\mathbf{r}_O$ is the position of non-magnetic ion (oxygen) and $\mathbf{r}_i$ the position of the spin $\mathbf{S}_i$ etc. These vectors are defined in Fig. 17a in the particular case where the displacements are in the xy plane. We have therefore $\mathbf{D}_{i,j}$ perpendicular to the xy plane in this case.

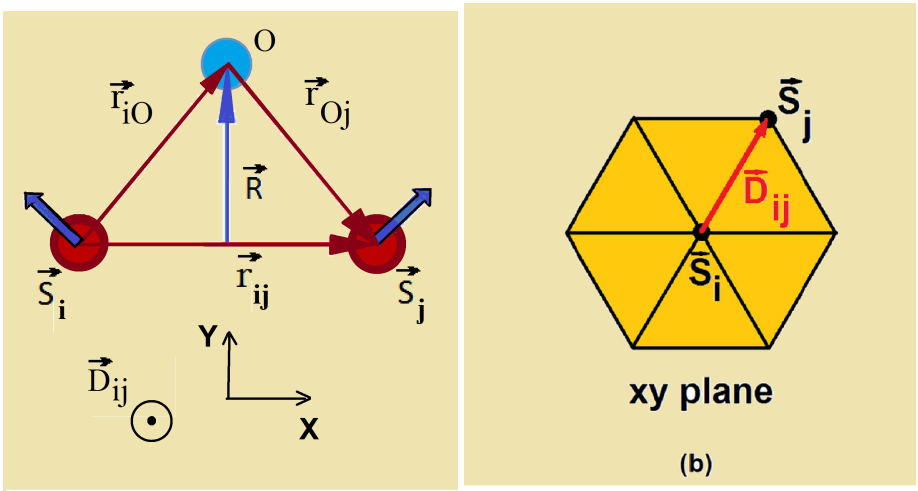

Figure 17. (a) D vector along the z direction perpendicular to the xy plane. See the definition of the D vector in the text, (b) In-plane $\mathbf{D}_{ij}$ vector chosen along the direction connecting spin $\mathbf{S}_i$ to spin $\mathbf{S}_j$ in the xy plane.

Note however that if the atom displacements are in 3D space, $\mathbf{D}_{i,j}$ can be in any direction. In this paper, we consider also the case where $\mathbf{D}_{i,j}$ lies in the xy plane as shown in Fig. 17b where $\mathbf{D}_{i,j}$ is taken along the vector connecting spin $\mathbf{S}_i$ to spin $\mathbf{S}_j$.

Note that from Eq. (54) one has

$$\mathbf{D}_{j,i} = -\mathbf{D}_{i,j} \tag{55}$$

Preprints (www.preprints.org) | NOT PEER-REVIEWED | Posted: 18 July 2022 doi:10.20944/preprints202207.0268.v1

In the case of perpendicular $\mathbf{D}_{i,j}$, let us define $\mathbf{u}_{i,j}$ as the unit vector on the z axis. From Eqs. (54)-(55) one writes

$$\begin{aligned} \mathbf{D}_{i,j} &= D\mathbf{u}_{i,j} && (56) \\ \mathbf{D}_{j,i} &= D\mathbf{u}_{j,i} = -D\mathbf{u}_{i,j} && (57) \end{aligned}$$

where D represents the DM interaction strength.

In the case of in-plane $\mathbf{D}_{i,j}$, we define $\mathbf{D}_{i,j}$ as

$$\mathbf{D}_{i,j} = D(\mathbf{r}_j - \mathbf{r}_i)/|\mathbf{r}_j - \mathbf{r}_i| = D\mathbf{r}_{ij} \quad (58)$$

where D is a constant and $\mathbf{r}_{ij}$ denotes the unit vector along $\mathbf{r}_j - \mathbf{r}_i$. The case of in-plane $\mathbf{D}_{i,j}$ on the frustrated triangular lattice (see Fig. 17b) has been recently studied since this case gives rise to a beautiful skyrmion crystal composed of three interpenetrating sublattice skyrmions in a perpendicular applied magnetic field.[44,47,48] A description of this case is however out of the purpose of this review.

5.2. Ground State with a Perpendicular $\mathbf{D}$ *in Zero Field*

The Hamiltonian is given by

$$\begin{aligned} \mathcal{H} &= -J\sum_{\langle ij\rangle}\mathbf{S_i}\cdot\mathbf{S_j} - D\sum_{\langle ij\rangle}\mathbf{u}_{i,j}\cdot\mathbf{S_i}\times\mathbf{S}_j \\ &\quad -H\sum_i S_i^z \end{aligned} \quad (59)$$

where $\mathbf{S_i}$ is a classical Heisenberg spin of magnitude 1 occupying the lattice site i. The first sum runs over all spin nearest-neighbor (NN) pairs with an antiferromagnetic exchange interaction J ($J < 0$), while the second sum is performed over all DM interactions between NN. H is the magnitude of a magnetic field applied along the z direction perpendicular to the lattice xy plane.

In the absence of J, unlike the bipartite square lattice where one can arrange the NN spins to be perpendicular with each order in the xy plane, the triangular lattice cannot fully satisfy the DM interaction for each bond, namely with the perpendicular spins at the ends. For this particular case of interest, we can analytically calculate the GS spin configuration as shown in the following. One considers a triangular plaquette with three spins numbered as 1, 2 and 3 embedded in the lattice. For convenience, in a hexagonal (or triangular) lattice, we define the three sublattices as follows: consider the up-pointing triangles (there are 3 in a hexagon, see the blue triangles in Fig. 18), for the first triangle one numbers in the counter-clockwise sense 1, 2, 3 then one does it for the other two up-pointing triangles of the hexagon, one sees that each lattice site belongs to a sublattice. The DM energy of a plaquette is written as

$$\begin{aligned} H_p &= -2D[\mathbf{u}_{1,2}\cdot\mathbf{S}_1\times\mathbf{S}_2 + \mathbf{u}_{2,3}\cdot\mathbf{S}_2\times\mathbf{S}_3 + \mathbf{u}_{3,1}\cdot\mathbf{S}_3\times\mathbf{S}_1] \\ &= -2D[\sin\theta_{1,2} + \sin\theta_{2,3} + \sin\theta_{3,1}] \end{aligned} \quad (60)$$

where the factor 2 of the D term takes into account the opposite neighbors outside the plaquette, and where $\theta_{1,2} = \theta_2 - \theta_1$ is the oriented angle between $\mathbf{S}_1$ and $\mathbf{S}_2$, etc. Note that the u vectors are in the same direction because we follow the counter-clockwise tour on the plaquette.

Preprints (www.preprints.org) | NOT PEER-REVIEWED | Posted: 18 July 2022 doi:10.20944/preprints202207.0268.v1

The minimization of H_p yields

$$\frac{dH_p}{d\theta_1} = 0 = -2D[-\cos(\theta_2-\theta_1)+\cos(\theta_1-\theta_3)] \quad (61)$$
$$\frac{dH_p}{d\theta_2} = 0 = -2D[\cos(\theta_2-\theta_1)-\cos(\theta_3-\theta_2)] \quad (62)$$
$$\frac{dH_p}{d\theta_3} = 0 = -2D[\cos(\theta_3-\theta_2)-\cos(\theta_1-\theta_3)] \quad (63)$$

The solutions for the above equations are

$$\theta_{1,2} = \theta_{3,1} \text{ so that } \theta_{3,2} = \theta_{3,1}+\theta_{1,2} = 2\theta_{1,2} \quad (64)$$
$$\theta_{2,3} = \theta_{1,2} \text{ so that } \theta_{1,3} = \theta_{1,2}+\theta_{2,3} = 2\theta_{2,3} \quad (65)$$
$$\theta_{3,1} = \theta_{2,3} \text{ so that } \theta_{2,1} = \theta_{2,3}+\theta_{3,1} = 2\theta_{3,1} \quad (66)$$

Note that the second and third lines can be obtained by the circular permutation of the indices 1,2 and 3 using the first line. These three equations, Eqs. (64)-(66), should be solved. There are more than one solution. We have from Eq. (61) $\cos(\theta_{1,2}) = \cos(\theta_{3,1})$. Using Eq. (66) one obtains

$$\cos(2\theta_{3,1}) = \cos(\theta_{3,1}) \quad \rightarrow 2\cos^2(\theta_{3,1}) - \cos(\theta_{3,1}) - 1 = 0 \quad (67)$$

This second-degree equation gives $\cos(\theta_{3,1}) = \frac{1\pm\sqrt{1+8}}{4}$. Only minus solution is acceptable so that $\theta_{3,1} = \theta_{2,3} = \pi/6$. From Eq. (66), one has $\theta_{2,1} = \pi/3$. This is one solution given by Eq. (68) below. Note that we have taken one of them, Eq. (66), to obtain explicit solutions for the three angles given in Eq. (68). We can do the same calculation starting with Eqs. (64)-(65) to get explicit solutions given in Eqs. (69)-(70). We note that when we make a circular permutation of the indices of Eq. (68) we get Eq. (69), and a circular permutation of Eq. (69) gives Eq. (70). One summarizes the three degenerate solutions below

$$\theta_{3,1} = \theta_{2,3} = \pi/6, \ \ \theta_{2,1} = \pi/3 \quad (68)$$
$$\theta_{1,2} = \theta_{3,1} = \pi/6, \ \ \theta_{3,2} = \pi/3 \quad (69)$$
$$\theta_{2,3} = \theta_{1,2} = \pi/6, \ \ \theta_{1,3} = \pi/3 \quad (70)$$

We show in Fig. 18 the spin orientations of the solution (68). The GS energy is obtained by replacing the angles into Eq. (60). For the three solutions, one gets the energy of the plaquette

$$H_p = -3D\sqrt{3} \quad (71)$$

We have three degenerate GSs.

Note that this solution can be numerically obtained by the steepest descent method described above. The result is shown in Fig. 19 for the full lattice. We see in the zoom that the spin configuration on a plaquette is what obtained analytically, with a global spin rotation as explained in the caption of Fig. 18.

As said above, to use the steepest-descent method, we consider a triangular lattice of lateral dimension L. The total number of sites N is given by $N = L \times L$. To avoid the finite size effect, we have to find the size limit beyond which the GS does not depend on the lattice size. This is found for $L \geq 100$. Most of calculations have been performed for $L = 100$.

5.3. Ground State with both perpendicular **D** *and J in Zero Field- Spin Waves*

When both J and perpendicular **D** are present, a compromise is established between these competing interactions. In zero field, the GS shows non-collinear but periodic in-plane spin

Preprints (www.preprints.org) | NOT PEER-REVIEWED | Posted: 18 July 2022 doi:10.20944/preprints202207.0268.v1

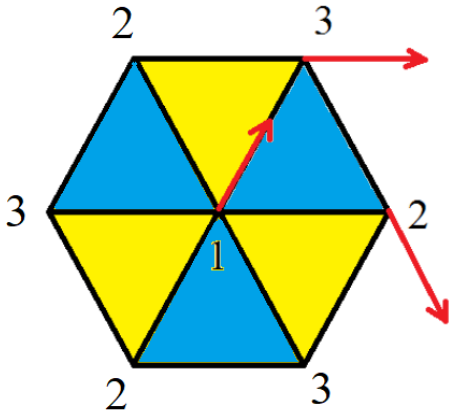

Figure 18. Perpendicular $\mathbf{D}_{i,j}$: Ground-state spin configuration with only Dzyaloshinskii-Moriya interaction on the triangular lattice ($J = 0$) is analytically determined. One angle is 120 degrees, the other two are 60 degrees. Note that the choice of the 120-degree angle in this figure is along the horizontal spin pair. This configuration is one GS, the other two GSs have the 120-degree angles on respectively the two diagonal spin pairs. Note also that the spin configuration is invariant under the global spin rotation in the xy plane. For convenience, the spins are decomposed into three sublattices numbered 1, 2 and 3. See text for explanation.

configurations. The planar spin configuration is easily understood: when **D** is perpendicular and without J, the spins are in the plane. When J is antiferromagnetic without **D**, the spins are also in the plane and form a 120-degree structure. When **D** and J exist together the angles between NN's change but they still in the plane in order to keep both D and J interactions as low as possible. An example is shown in Fig. 20 where one sees that the GS is planar and characterized by two angles $\theta = 102$ degrees and one angle $\beta = 156$ degrees formed by three spins on a triangle plaquette. Note that there are three degenerate states where β is chosen for the pair (1,2) (Fig. 20a) or the pair (2,3) or the pair (3,1). Changing the value of D will change the angle values. Changing the sign of D results in a change of the sense of the chirality, but not the angle values.

In the case of perpendicular $\mathbf{D}_{i,j}$ in zero-field, as shown above we find the GS on a hexagon of the lattice is defined by four identical angles β and two angles θ as shown in Fig. 20. The values of β and θ depend on the value of D. We take $J = -1$ (antiferromagnetic) hereafter. For $D = 0.5$ we have $\beta = 156$ degrees and $\theta = 102$ degrees. For $D = 0.4$ we obtain $\beta = 108$ degrees and $\theta = 144$ degrees, using $N = 60 \times 60$.

The periodicity of the GS allows us to calculate the SW spectrum in the following.

The model for the calculation of the SW spectrum uses quantum Heisenberg spins of magnitude $1/2$, it is given by

$$\mathcal{H} = -J \sum_{\langle i,j \rangle} \mathbf{S_i} \cdot \mathbf{S_j} - D \sum_{\langle i,j \rangle} \mathbf{u}_{i,j} \cdot \mathbf{S_i} \times \mathbf{S_j} - I \sum_{\langle i,j \rangle} S_i^z \, S_j^z \cos\theta_{ij} \tag{72}$$

where θ_{ij} is the angle between $\mathbf{S_i}$ and $\mathbf{S_j}$ and the last term is an extremely small anisotropy added to stabilize the SW when the wavelength k tends to zero [31,40]. Note that $\mathbf{u}_{i,j}$ points up and down along the z axis for respective two opposite neighbors.

Preprints (www.preprints.org) | NOT PEER-REVIEWED | Posted: 18 July 2022 doi:10.20944/preprints202207.0268.v1

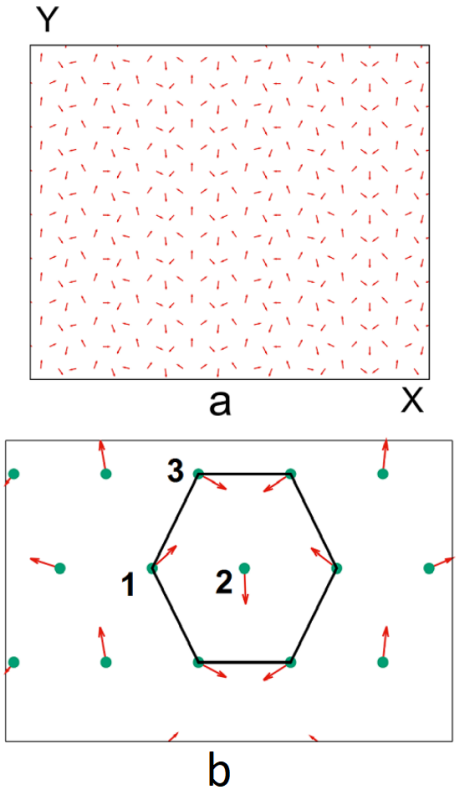

Figure 19. Perpendicular $\mathbf{D}_{i,j}$: (a) Ground-state spin configuration with only Dzyaloshinskii-Moriya interaction on the triangular lattice ($J = 0$) obtained numerically by the steepest descent method, (b) a zoom on a hexagonal cell, this is exactly what obtained analytically shown in Fig. 18 with a global spin rotation in the xy plane: the angle of the horizontal pair (1,2) is 120 degrees, those of (2,3) and (3,1) are equal to 60 degrees.

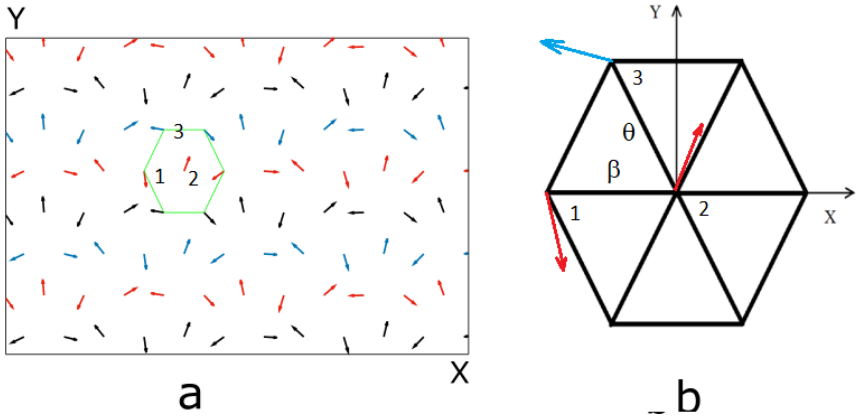

Figure 20. Perpendicular $\mathbf{D}_{i,j}$ with antiferromagnetic J: (a) Ground-state spin configuration in zero field for $D = 0.5$, $J = -1$ where the angles in a hexagon are shown in (b) with $\beta = 156$ degrees for the pair (1,2) on the horizontal axis and $\theta = 102$ degrees for the pairs (2,3) and (3,1) on the diagonals. Note that there are two other degenerate states where β is chosen for the pair (2,3) or (3,1).

As before, in order to calculate the SW spectrum for systems of non-collinear spin configurations, we have to use the system of local coordinates. The Hamiltonian becomes

Preprints (www.preprints.org) | NOT PEER-REVIEWED | Posted: 18 July 2022 doi:10.20944/preprints202207.0268.v1

$$\begin{aligned}\mathcal{H} = &- J\sum_{\langle i,j\rangle}\frac{1}{4}(S_i^+S_j^+ + S_i^-S_j^-)(\cos\theta_{ij}-1) + \frac{1}{4}(S_i^+S_j^- + S_i^-S_j^+)(\cos\theta_{ij}+1)\\ &+ \frac{1}{2}S_j^z\sin\theta_{ij}(S_i^+ + S_i^-) - \frac{1}{2}\sin\theta_{ij}S_i^z(S_J^+ + S_j^-) + S_i^zS_j^z\cos\theta_{ij}\\ &- D\sum_{\langle i,j\rangle}S_i^zS_j^z\sin\theta_{i,j} + \frac{1}{4}\sin\theta_{i,j}(S_i^+S_j^+ + S_i^+S_j^- + S_i^-S_j^+) + \frac{1}{2}\cos\theta_{i,j}(S_i^z(S_j^+ + S_j^-) - S_j^z(S_i^+ + S_i^-))\\ &- I\sum_{\langle i,j\rangle}S_i^z\,S_j^z\cos\theta_{i,j}\end{aligned}$$

We define the two GFs by Eqs. (11)-(12) and use the equations of motion of these functions (13)-(14), we obtain

$$\begin{aligned}i\hbar\frac{dG_{i,j}(t-t')}{dt} &= 2<S_i^z>\delta_{i,j}\delta(t-t') - J\sum_{\langle l\rangle}<S_i^z>F_{l,j}(t-t')(\cos\theta_{i,l}-1)\\ &+ <S_i^z>G_{l,j}(t-t')(\cos\theta_{i,l}+1) - 2\cos\theta_{i,l}<S_l^z>G_{i,j}(t-t')\\ &+ D\sum_{\langle l\rangle}2\sin\theta_{i,l}<S_i^z>F_{l,j}(t-t') - \sin\theta_{i,l}<S_i^z>(G_{l,j}(t-t') + F_{l,j}(t-t'))\\ &- 2I\sum_{\langle l\rangle}\cos\theta_{i,l}<S_i^z>F_{l,j}(t-t')\end{aligned}$$

$$\begin{aligned}i\hbar\frac{dF_{i,j}(t-t')}{dt} &= J\sum_{\langle l\rangle}<S_i^z>G_{l,j}(t-t')(\cos\theta_{i,l}-1)\\ &+ <S_i^z>F_{l,j}(t-t')(\cos\theta_{i,l}+1) - 2\cos\theta_{i,l}<S_l^z>F_{i,j}(t-t')\\ &- D\sum_{\langle l\rangle}2\sin\theta_{i,l}<S_i^z>G_{l,j}(t-t') - \sin\theta_{i,l}<S_i^z>(G_{l,j}(t-t') + F_{l,j}(t-t'))\\ &+ 2I\sum_{\langle l\rangle}\cos\theta_{i,l}<S_i^z>G_{l,j}(t-t')\end{aligned}$$

Note that $<S_i^z>$ is the average of the spin i on its local quantization axis in the local-coordinates system (see Ref. [38]). We use now the time Fourier transforms of the G and F, we get

$$\begin{aligned}\hbar\omega g_{i,j} &= 2\mu_i\delta_{i,j} - J\sum_{\langle l\rangle}\mu_i f_{lj}e^{-i\mathbf{k}\cdot(\mathbf{R}_i-\mathbf{R}_l)}(\cos\theta_{i,l}-1)\\ &+ \mu_i g_{lj}e^{-i\mathbf{k}\cdot(\mathbf{R}_i-\mathbf{R}_l)}(\cos\theta_{i,l}+1) - 2\mu_l\cos\theta_{i,l}g_{i,j}\\ &- D\sum_{\langle l\rangle}2\sin\theta_{i,l}\mu_l g_{i,j} - \sin\theta_{i,l}\mu_i(g_{l,j}e^{-i\mathbf{k}\cdot(\mathbf{R}_i-\mathbf{R}_l)} + f_{l,j}e^{-i\mathbf{k}\cdot(\mathbf{R}_i-\mathbf{R}_l)})\\ &+ 2I\sum_{\langle l\rangle}\mu_l\cos\theta_{i,l}g_{i,j}\end{aligned} \tag{73}$$

and

$$\begin{aligned}\hbar\omega f_{i,j} &= J\sum_{\langle l\rangle}\mu_i g_{lj}e^{-i\mathbf{k}\cdot(\mathbf{R}_i-\mathbf{R}_l)}(\cos\theta_{i,l}-1)\\ &+ \mu_i f_{lj}e^{-i\mathbf{k}\cdot(\mathbf{R}_i-\mathbf{R}_l)}(\cos\theta_{i,l}+1) - 2\mu_l\cos\theta_{i,l}f_{i,j}\\ &+ D\sum_{\langle l\rangle}2\sin\theta_{i,l}\mu_l f_{i,j} - \sin\theta_{i,l}\mu_i(g_{l,j}e^{-i\mathbf{k}\cdot(\mathbf{R}_i-\mathbf{R}_l)} + f_{l,j}e^{-i\mathbf{k}\cdot(\mathbf{R}_i-\mathbf{R}_l)})\\ &- 2I\sum_{\langle l\rangle}\mu_l\cos\theta_{i,l}f_{i,j}\end{aligned} \tag{74}$$

Preprints (www.preprints.org) | NOT PEER-REVIEWED | Posted: 18 July 2022 doi:10.20944/preprints202207.0268.v1

where $\mu_i \equiv < S_i^z >$, $\mathbf{k}$ is the wave vector in the reciprocal lattice of the triangular lattice, and ω the SW frequency. Note that the index z in S_i^z is not referred to the real space direction z, but to the quantization axis of the spin $\mathbf{S}_i$. At this stage, we have to replace $\theta_{i,j}$ by either β or θ according on the GS spin configuration given above (see Fig. 20).

As in the previous sections, writing the above equations under a matrix form, we have

$$\mathbf{M}(\hbar\omega)\,\mathbf{h} = \mathbf{C}, \tag{75}$$

where $\mathbf{M}(\hbar\omega)$ is a square matrix of dimension 2×2, $\mathbf{h}$ and $\mathbf{C}$ are the column matrices which are defined as follows

$$\mathbf{h} = \begin{pmatrix} g_{i,j} \\ f_{i,j} \end{pmatrix}, \qquad \mathbf{C} = \begin{pmatrix} 2\langle S_i^z \rangle \delta_{i,j} \\ 0 \end{pmatrix}, \tag{76}$$

and the matrix $\mathbf{M}(\hbar\omega)$ is given by

$$\mathbf{M}(\hbar\omega) = \begin{pmatrix} \hbar\omega + A & B \\ -B & \hbar\omega - A \end{pmatrix}$$

The nontrivial solution of g and f imposes the following secular equation:

$$0 = \begin{pmatrix} \hbar\omega + A & B \\ -B & \hbar\omega - A \end{pmatrix} \tag{77}$$

where

$$\begin{aligned} A = &-J(8\mu_i \cos\beta(1+I) + 4\mu_i \cos\theta(1+I) - 4\mu_i\gamma(\cos\beta + 1) - 2\mu_i\alpha(\cos\theta + 1)) \\ &- D(4\mu_i \sin\beta\gamma + 2\mu_i \sin\theta\alpha) + D(8\mu_i \sin\beta + 4\mu_i \sin\theta) \end{aligned} \tag{78}$$

$$B = J(4\mu_i\gamma(\cos\beta - 1) + 2\mu_i\alpha(\cos\theta - 1)) - D(4\gamma\mu_i \sin\beta + 2\mu_i\alpha \sin\theta) \tag{79}$$

where the sum on the two NN on the x axis (see Fig. 20b) is

$$\sum_l e^{-i\mathbf{k}\cdot(\mathbf{R}_i - \mathbf{R}_l)} = 2\cos(k_x) \equiv 2\alpha \tag{80}$$

and the sum on the four NN on the oblique directions of the hexagon (see Fig. 20b) is

$$\sum_l e^{-i\mathbf{k}\cdot(\mathbf{R}_i - \mathbf{R}_l)} = 4\cos(k_x/2)\ \cos(\sqrt{3}k_y/2) \equiv 4\gamma \tag{81}$$

Solving Eq. (77) for each given (k_x, k_y) one obtains the SW frequency $\omega(k_x, ky)$:

$$(\hbar\omega)^2 = A^2 - B^2 \ \ \rightarrow \hbar\omega = \pm\sqrt{A^2 - B^2} \tag{82}$$

Plotting $\omega(k_x, ky)$ in the space (k_x, ky) one obtains the full SW spectrum.

The spin length $\langle S_i^z \rangle$ (for all i, by symmetry) is given by (see technical details in Ref. [31]):

$$\langle S^z \rangle \equiv \langle S_i^z \rangle = \frac{1}{2} - \frac{1}{\Delta} \int\int dk_x dk_z \sum_{i=1}^{2} \frac{Q(E_i)}{e^{E_i/k_B T} - 1} \tag{83}$$

where $E_i (i = 1, 2) = \pm\sqrt{A^2 - B^2}$ are the two solutions given above, and $Q(E_i)$ is the determinant (cofactor) obtained by replacing the first column of $\mathbf{M}$ by $\mathbf{C}$ at E_i.

The spin length $\langle S^z \rangle$ at a given T is calculated self-consistently by following the method given in Ref. [31,38].

Let us show the SW spectrum ω (taking $\hbar = 1$) for the case of $J = -1$ and $D = 0.5$ in Fig. 21 versus k_y with $k_x = 0$ (Fig. 21a) and versus k_x for $k_y = 0$ (Fig. 21b). In order to see the effect of

Preprints (www.preprints.org) | NOT PEER-REVIEWED | Posted: 18 July 2022 doi:10.20944/preprints202207.0268.v1

the DM interaction alone we take the anisotropy $I = 0$. One observes here that for a range of small wave-vectors the SW frequency is imaginary. The SW corresponding to these modes do not propagate in the system. Why do we have this case here? The answer is that when the NN make a large angle (perpendicular NN, for example), one cannot define a wave vector in that direction. Physically, when k is small the B coefficient is larger than A in Eq. (82) giving rise to imaginary ω. Note that the anisotropy I is contained in A so that increasing I for small k will result in $A > B$ making ω real.

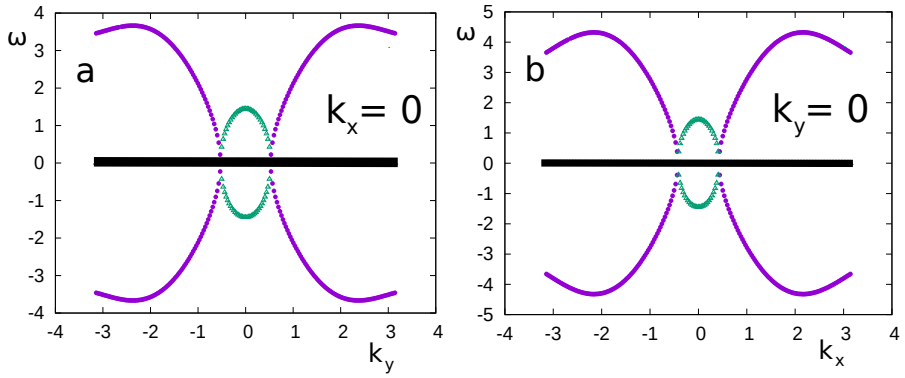

Figure 21. (a) Spin-wave spectrum versus k_y with $k_x = 0$ at $T = 0$ for $I = 0$, (b) Spin-wave spectrum versus k_x with $k_y = 0$ at $T = 0$ for $I = 0$. The magenta curves show the real frequency, while the green ones show the imaginary frequency. See text for comments. Parameters: $D = 0.5$, $J = -1$, $H = 0$ where $\theta = 102$ degrees and $\beta = 156$ degrees (see the spin configuration shown in Fig. 20), $\hbar = 1$.

We show now in Fig. 22a the spectrum along the axis $k_x = k_y$ at $T = 0$ for $I = 0$. Again here the frequency is imaginary for small k, as in the previous figure. The spin length $< S^z >$ along the local quantization axis is shown in Fig. 22b. Several remarks are in order: i) At $T = 0$, the spin length is not equal to $1/2$ as in ferromagnets because of the zero-point spin contraction due to antiferromagnetic interactions (see Ref. [31]), its length is $\simeq 0.40$, quite small; ii) the magnetic ordering is destroyed at $T \simeq 1.2$.

To close the present section, we note that in the case of perpendicular **D** considered above, we did not observe skyrmion textures when applying a perpendicular magnetic field: all spin configurations are no more planar, making the calculation of the SW spectrum more difficult. This problem is left for a future investigation.

6. Other systems of non-collinear ground-state spin configurations: frustrated surface in stacked triangular thin films

In this section, we study by the GF method effects of a frustrated surface on the properties of thin films made of stacked triangular layers of atoms bearing quantum Heisenberg spins. We suppose that the in-plane surface interaction J_s can be antiferromagnetic or ferromagnetic while all other interactions are ferromagnetic. We show that the GS spin configuration is non collinear when J_s is lower than a critical value J_s^c. The film surfaces are then frustrated. In the frustrated case, there are two phase transitions related to disorderings of surface and interior layers. The GF results agree qualitatively with Monte Carlo simulation using the classical spins (see the original paper in Ref.).

Preprints (www.preprints.org) | NOT PEER-REVIEWED | Posted: 18 July 2022 doi:10.20944/preprints202207.0268.v1

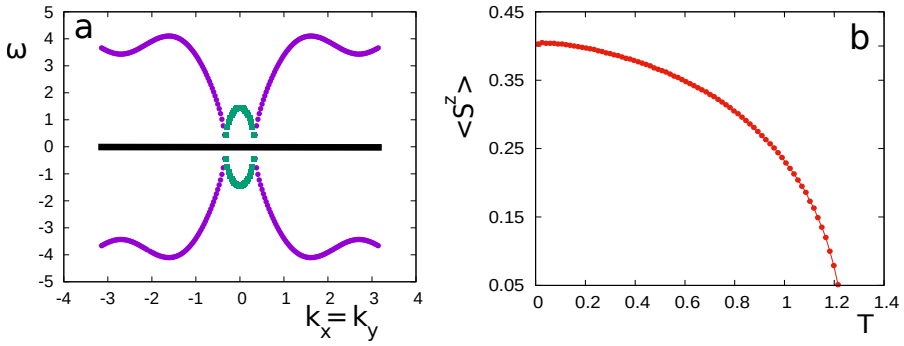

Figure 22. (a) Spin-wave spectrum versus $k_x = k_y$ at $T = 0$ for $I = 0$. The magenta curves show the real frequency, while the green ones show the imaginary frequency. See text for comments, (b) The spin length S^z versus temperature T ($k_B = 1$). Parameters: $D = 0.5$, $J = -1$, $H = 0$ where $\theta = 102$ degrees and $\beta = 156$ degrees (see the spin configuration shown in Fig. 20).

In this section we review some ot the results given in the original paper Ref. [39], emphasizing the SW calculation and the important results. The Hamiltonian is given by

$$\mathcal{H} = -\sum_{\langle i,j \rangle} J_{i,j} \mathbf{S}_i \cdot \mathbf{S}_j - \sum_{<i,j>} I_{i,j} S_i^z S_j^z \tag{84}$$

where $\mathbf{S}_i$ is the Heisenberg spin at the lattice site i, $\sum_{\langle i,j \rangle}$ indicates the sum over the NN spin pairs $\mathbf{S}_i$ and $\mathbf{S}_j$. The last term, which will be taken to be very small, is needed to make the film with a finite thickness to have a phase transition at a finite temperature in the case where all exchange interactions $J_{i,j}$ are ferromagnetic. This guarantees the existence of a phase transition at finite temperature, since it is known that a strictly two-dimensional system with an isotropic non-Ising spin model (XY or Heisenberg model) does not have long-range ordering at finite temperature.[40]

Interaction between two NN surface spins is equal to J_s. Interaction between layers and interaction between NN in interior layers are supposed to be ferromagnetic and all equal to $J = 1$ for simplicity. The two surfaces of the film are frustrated if J_s is antiferromagnetic ($J_s < 0$).

6.1. Ground state

For $J_s > 0$ (ferromagnetic interaction), the magnetic GS is ferromagnetic. However, when J_s is negative the surface spins are frustrated. If the surface is deconnected with the beneath layer, the surface spins form the famous 120-degree structure because of the antiferromagnetic interaction on the surface plane. Now when we turn on the ferromagnetic interaction with the second layer, there is a competition between the non collinear surface ordering and the ferromagnetic ordering due to the ferromagnetic interaction with the interior spins.

We first determine the GS configuration for $I = I_s = 0.1$ by using the steepest descent method : starting from a random spin configuration, we calculate the magnetic local field at each site and align the spin of the site in its local field. In doing so for all spins and repeat until the convergence is reached, we obtain in general the GS configuration, without metastable states in the present model. The result shows that when J_s is negative and smaller than a critical value J_s^c the magnetic GS is obtained from pulling out the planar 120° spin structure along the z axis by an angle β. The three spins on a triangle on the surface form thus an 'umbrella' with an angle α between them and an angle β between a surface spin and its beneath neighbor (see Fig. 23). This non planar structure is due to the interaction of the

Preprints (www.preprints.org) | NOT PEER-REVIEWED | Posted: 18 July 2022 doi:10.20944/preprints202207.0268.v1

spins on the beneath layer, just like an external applied field applied in the z direction. Of course, when J_s is larger than J_s^c one has the collinear ferromagnetic GS as expected: the frustration is not strong enough to resist the ferromagnetic interaction from the beneath layer.

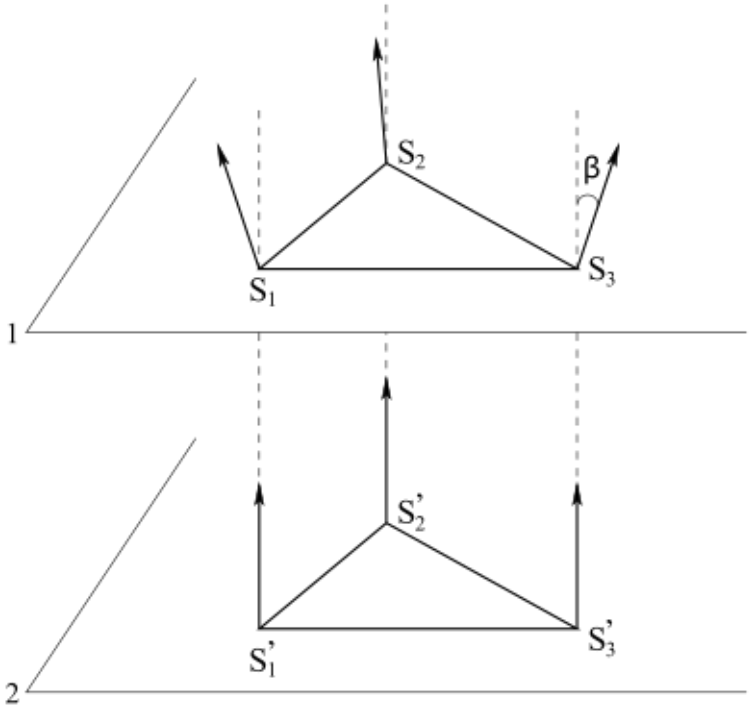

Figure 23. Non collinear surface spin configuration. Angles between spins on layer 1 are all equal (noted α), while angles between vertical spins are β.

We show in Fig. 24 $\cos(\alpha)$ and $\cos(\beta)$ as functions of J_s. The critical value J_s^c is found between -0.18 and -0.19. This value can be calculated analytically by assuming the 'umbrella structure'. For GS analysis, it suffices to consider just a cell shown in Fig.23. This is justified by the numerical determination discussed above. Furthermore, we consider as a single solution all configurations obtained from each other by any global spin rotation.

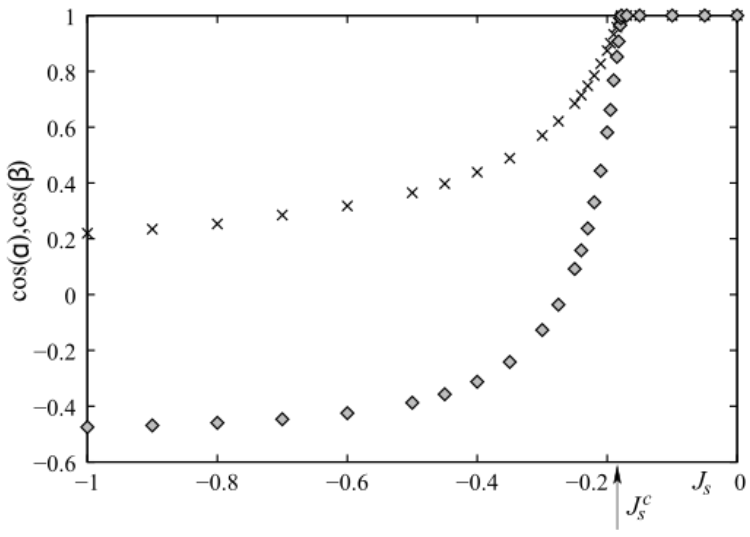

Figure 24. Ground state determined by $\cos(\alpha)$ (diamonds) and $\cos(\beta)$ (crosses) as functions of J_s. Critical value of J_s^c is shown by the arrow.

Preprints (www.preprints.org) | NOT PEER-REVIEWED | Posted: 18 July 2022 doi:10.20944/preprints202207.0268.v1

Let us consider the full Hamiltonian (84). For simplicity, the interaction inside the surface layer is set equal J_s $(-1 \leq J_s \leq 1)$ and all others are set equal to $J > 0$. Also, we suppose that $I_{i,j} = I_s$ for spins on the surfaces with the same sign as J_s and all other $I_{i,j}$ are equal to $I > 0$ for the inside spins including interaction between a surface spin and the spin on the beneath layer.

The spins are numbered as in Fig. 23: S_1, S_2 and S_3 are the spins in the surface layer (first layer), S'_1, S'_2 and S'_3 are the spins in the internal layer (second layer). The Hamiltonian for the cell is written as

$$\begin{aligned} H_p &= -6\left[J_s\left(\mathbf{S}_1\cdot\mathbf{S}_2+\mathbf{S}_2\cdot\mathbf{S}_3+\mathbf{S}_3\cdot\mathbf{S}_1\right)\right. \\ &\quad \left.+I_s\left(S_1^zS_2^z+S_2^zS_3^z+S_3^zS_1^z\right)\right. \\ &+ \left. J\left(\mathbf{S}'_1\cdot\mathbf{S}'_2+\mathbf{S}'_2\cdot\mathbf{S}'_3+\mathbf{S}'_3\cdot\mathbf{S}'_1\right)\right. \\ &\quad \left.+I\left(S_1'^zS_2'^z+S_2'^zS_3'^z+S_3'^zS_1'^z\right)\right] \\ &- 2J\left(\mathbf{S}_1\cdot\mathbf{S}'_1+\mathbf{S}_2\cdot\mathbf{S}'_2+\mathbf{S}_3\cdot\mathbf{S}'_3\right) \\ &\quad -2I\left(S_1^zS_1'^z+S_2'^zS_2'^z+S_3^zS_3'^z\right), \end{aligned} \tag{85}$$

We decompose now each spin into two components: an xy component, which is a vector, and a z component $\mathbf{S}_i = (\mathbf{S}_i^{\parallel}, S_i^z)$. Only surface spins have xy vector components. The angle between these xy components of NN surface spins is $\gamma_{i,j}$ which is in fact the projection of α defined above on the xy plane. By symmetry, we have

$$\gamma_{1,2} = 0,\ \gamma_{2,3} = \frac{2\pi}{3},\ \gamma_{3,1} = \frac{4\pi}{3}. \tag{86}$$

The angles β_i and β'_i of the spin $\mathbf{S}_i$ and $\mathbf{S}'_i$ with the z axis are by symmetry

$$\begin{cases} \beta_1 = \beta_2 = \beta_3 = \beta, \\ \beta'_1 = \beta'_2 = \beta'_3 = 0, \end{cases}$$

The total energy of the cell (85), with $S_i = S'_i = \frac{1}{2}$, can be rewritten as

$$\begin{aligned} H_p &= -\frac{9(J+I)}{2} - \frac{3(J+I)}{2}\cos\beta - \frac{9(J_s+I_s)}{2}\cos^2\beta \\ &+ \frac{9J_s}{4}\sin^2\beta. \end{aligned} \tag{87}$$

By a variational method, the minimum of the cell energy corresponds to

$$\frac{\partial H_p}{\partial\beta} = \left(\frac{27}{2}J_s + 9I_s\right)\cos\beta\sin\beta + \frac{3}{2}(J+I)\sin\beta = 0 \tag{88}$$

We have

$$\cos\beta = -\frac{J+I}{9J_s+6I_s}. \tag{89}$$

For given values of I_s and I, we see that the solution (89) exists for $J_s \leq J_s^c$ where the critical value J_s^c is determined by $-1 \leq \cos\beta \leq 1$. For $I = -I_s = 0.1$, $J_s^c \approx -0.1889J$ in excellent agreement with the numerical results obtained from the steepest-descent method.

Preprints (www.preprints.org) | NOT PEER-REVIEWED | Posted: 18 July 2022 doi:10.20944/preprints202207.0268.v1

Now, using the GF method for such a film in the way described in the previous sections, we obtain the full Hamiltonian (84) in the local framework:

$$\begin{aligned}\mathcal{H} &= -\sum_{<i,j>} J_{i,j}\Big\{\frac{1}{4}\left(\cos\theta_{ij}-1\right)\left(S_i^+S_j^+ + S_i^-S_j^-\right)\\ &+ \frac{1}{4}\left(\cos\theta_{ij}+1\right)\left(S_i^+S_j^- + S_i^-S_j^+\right)\\ &+ \frac{1}{2}\sin\theta_{ij}\left(S_i^+ + S_i^-\right)S_j^z - \frac{1}{2}\sin\theta_{ij}S_i^z\left(S_j^+ + S_j^-\right)\\ &+ \cos\theta_{ij}S_i^zS_j^z\Big\} - \sum_{<i,j>} I_{i,j}S_i^zS_j^z \end{aligned} \tag{90}$$

where $\cos\left(\theta_{ij}\right)$ is the angle between two NN spins. We define the two coupled GF, and we write their equations of motions in the real space. Taking the Tyablikov's decoupling scheme to reduce higher-order GFs, and then using the Fourier transform in the xy plane we arrive at a matrix equation as in the previous section with the matrix $\mathbf{M}$ is defined as

$$\mathbf{M}\left(\omega\right) = \begin{pmatrix} A_1^+ & B_1 & D_1^+ & D_1^- & \cdots \\ -B_1 & A_1^- & -D_1^- & -D_1^+ & \vdots \\ \vdots & \cdots & \cdots & \cdots & \vdots \\ \vdots & C_{N_z}^+ & C_{N_z}^- & A_{N_z}^+ & B_{N_z} \\ \cdots & -C_{N_z}^- & -C_{N_z}^+ & -B_{N_z} & A_{N_z}^- \end{pmatrix}, \tag{91}$$

where

$$\begin{aligned} A_n^\pm &= \omega \pm \Big[\frac{1}{2}J_n\left\langle S_n^z\right\rangle\left(Z\gamma\right)\left(\cos\theta_n+1\right)\\ &- J_n\left\langle S_n^z\right\rangle Z\cos\theta_n - J_{n,n+1}\left\langle S_{n+1}^z\right\rangle\cos\theta_{n,n+1}\\ &- J_{n,n-1}\left\langle S_{n-1}^z\right\rangle\cos\theta_{n,n-1} - ZI_n\left\langle S_n^z\right\rangle\\ &- I_{n,n+1}\left\langle S_{n+1}^z\right\rangle - I_{n,n-1}\left\langle S_{n-1}^z\right\rangle\Big], \end{aligned} \tag{92}$$

$$B_n = \frac{1}{2}J_n\left\langle S_n^z\right\rangle\left(\cos\theta_n-1\right)\left(Z\gamma\right), \tag{93}$$

$$C_n^\pm = \frac{1}{2}J_{n,n-1}\left\langle S_n^z\right\rangle\left(\cos\theta_{n,n-1}\pm 1\right), \tag{94}$$

$$D_n^\pm = \frac{1}{2}J_{n,n+1}\left\langle S_n^z\right\rangle\left(\cos\theta_{n,n+1}\pm 1\right), \tag{95}$$

in which, $Z=6$ is the number of in-plane NN, $\theta_{n,n\pm1}$ the angle between two NN spins belonging to the layers n and $n\pm1$, θ_n the angle between two in-plane NN in the layer n, and

$$\gamma = \left[2\cos\left(k_xa\right) + 4\cos\left(k_ya/2\right)\cos\left(k_ya\sqrt{3}/2\right)\right]/Z.$$

Here, for compactness we have used the following notations:

i) J_n and I_n are the in-plane interactions. In the present model J_n is equal to J_s for the two surface layers and equal to J for the interior layers. All I_n are set to be I.

ii) $J_{n,n\pm1}$ and $I_{n,n\pm1}$ are the interactions between a spin in the n^{th} layer and its neighbor in the $(n\pm1)^{th}$ layer. Of course, $J_{n,n-1}=I_{n,n-1}$=0 if $n=1$, $J_{n,n+1}=I_{n,n+1}$=0 if $n=N_z$.

Solving $\det|\mathbf{M}|=0$, we obtain the SW spectrum ω of the present system.

For numerical calculation, we used $I=0.1J$ with $J=1$. For positive J_s, we take $I_s=0.1$ and for negative J_s, we use $I_s=-0.1$. A size of 80^3 points in the first Brillouin zone is used for numerical

Preprints (www.preprints.org) | NOT PEER-REVIEWED | Posted: 18 July 2022 doi:10.20944/preprints202207.0268.v1

integration. We start the self-consistent calculation from $T = 0$ with a small step for temperature 5×10^{-3} or 10^{-1} (in units of J/k_B). The convergence precision has been fixed at the fourth figure of the values obtained for the layer magnetizations.

6.2. Phase transition and phase diagram of the quantum case

We first show an example where $J_s = -0.5$ in Fig. 25. As seen, the surface-layer magnetization is much smaller than the second-layer one. In addition there is a strong spin contraction at $T = 0$ for the surface layer. This is due to the antiferromagnetic nature of the in-plane surface interaction J_s. One sees that the surface becomes disordered at a temperature $T_1 \simeq 0.2557$ while the second layer remains ordered up to $T_2 \simeq 1.522$. Therefore, the system is partially disordered for temperatures between T_1 and T_2. This result is very interesting because it confirms again the existence of the partial disorder in quantum spin systems observed earlier in bulk frustrated quantum spin systems.[50,51] Note that between T_1 and T_2, the ordering of the second layer acts as an external field on the first layer, inducing therefore a small value of its magnetization.

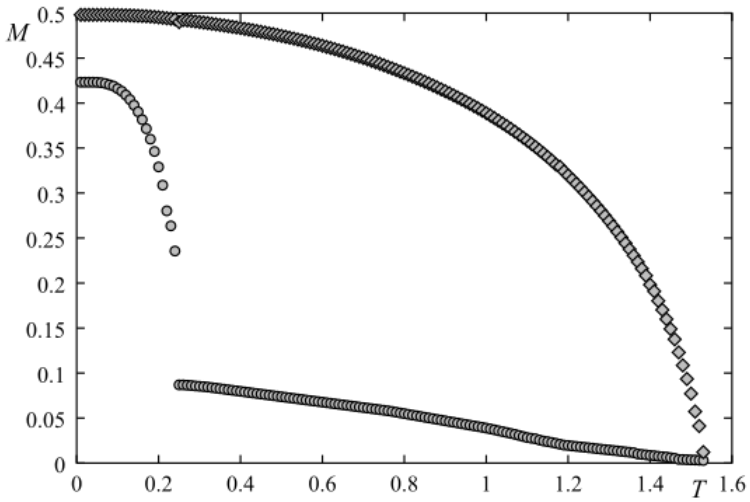

Figure 25. First two layer-magnetizations obtained by the Green function technique vs. T for $J_s = -0.5$ with $I = -I_s = 0.1$. The surface-layer magnetization (lower curve) is much smaller than the second-layer one. See text for comments.

We show in Fig. 26 the phase diagram in the space (J_s, T). Phase I denotes the surface canted-spin state, phase II indicates the ordered state, and phase III is the paramagnetic phase. Note that the surface transition does not exist separately for $J_s \geq J_s^c$.

6.3. Monte Carlo results

In this paragraph, we show the results obtained by MC simulations with the Hamiltonian 28 but the spins are the classical Heisenberg model of magnitude $S = 1$. This is to compare with the quantum case shown above.

The film sizes are $N \times N \times N_z$ where N_z is the number of layers (film thickness). We use here $N = 24, 36, 48, 60$ and $N_z = 4$ as in the quantum case presented above. Periodic boundary conditions are used in the XY planes. The equilibrating time is about 10^6 MC steps per spin and the averaging time is 2×10^6 MC steps per spin. $J = 1$ is taken as unit of energy in the following.

In Fig. 27 we show a frustrated case where $J_s = -0.5$. The surface layer in this case becomes disordered at a temperature much lower than that for the second layer. Note that the surface magnetization is not saturated to 1 at $T = 0$. This is because the surface spins make an angle with the z axis so their z component is less than 1 in the GS.

Preprints (www.preprints.org) | NOT PEER-REVIEWED | Posted: 18 July 2022 doi:10.20944/preprints202207.0268.v1

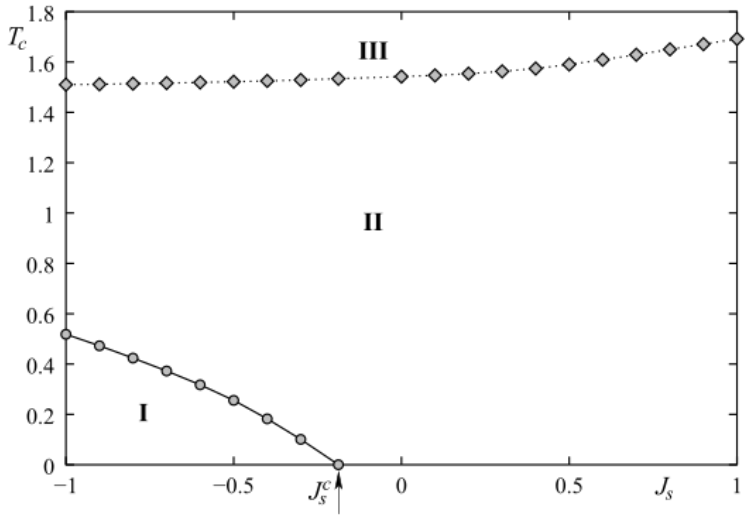

Figure 26. Phase diagram in the space (J_s, T) for the quantum Heisenberg model with $N_z = 4$, $I = |I_s| = 0.1$. See text for the description of phases I to III.

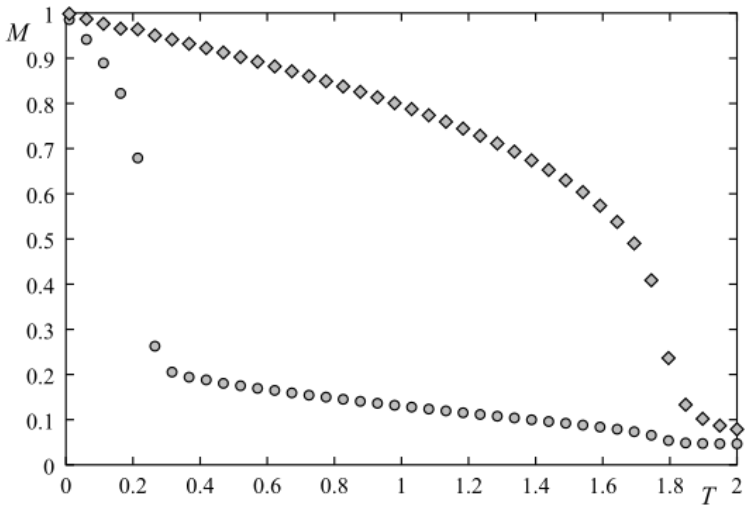

Figure 27. Magnetizations of layer 1 (circles) and layer 2 (diamonds) versus temperature T in unit of J/k_B for $J_s = -0.5$ with $I = -I_s = 0.1$.

Figure 28 shows the phase diagram obtained in the space (J_s, T). It is interesting to note that this phase diagram resembles remarkably to that obtained for the quantum counterpart model shown in Fig. 26. The difference in the values of the transition temperatures is due to the quantum and classical spins.

To close this review, we should mention a few works works where SW in the regime of non-collinear spin configurations have been studied: the frustration effects in antiferromagnetic face-centered cubic Heisenberg films have been studied in Ref. [49], a frustrated ferrimagnet in Ref. [50] and a quantum frustrated spin system in Ref. [51]. These results are not reviewed here to limit the paper's length. We refer the reader to those works for details.

7. Concluding remarks

As said in the Introduction, the self-consistent Green's function theory is the only one which allows to calculate the SW dispersion relation in the case of non-collinear spin configurations, in 2D and 3D as well as in thin films. The non-collinear spin configurations are due to the competition between different kinds of exchange interaction, to the geometry frustration, to the competition between ferromagnetic

Preprints (www.preprints.org) | NOT PEER-REVIEWED | Posted: 18 July 2022 doi:10.20944/preprints202207.0268.v1

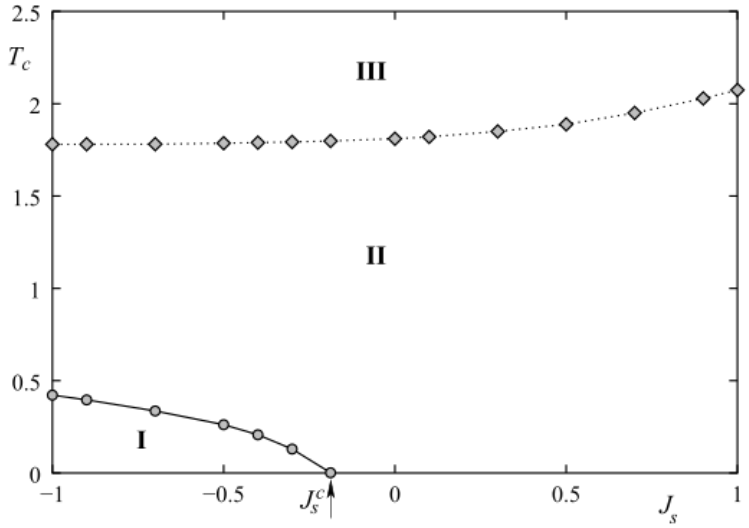

Figure 28. Phase diagram in the space (J_s, T) for the classical Heisenberg model with $N_z = 4$, $I = |I_s| = 0.1$. Phases I to III have the same meanings as those in Fig. 26 .

and/or antiferromagnetic interactions and the Dzyaloshinskii-Moriya interaction. We have shown that in the absence of an applied magnetic field, the GS spin configuration is non collinear but periodic in space. We have in most cases analytically calculated them. We have checked them by using the numerical steepest-descent method which consists in minimizing the local energy iteratively. The agreement between the analytical method and the numerical energy minimization is excellent. The determination of the GS is necessary because we need them to calculate the SW spectrum: SW are elementary excitations of the GS when T increases.

The double-fold purpose of this review is to show the method and the interest of its results. We have reviewed a selected number of works according to their interest of the community: helimagnets, materials with the Dzyaloshinskii-Moriya interaction, and the surface effects in thin magnetic films. The Dzyaloshinskii-Moriya interaction gives rise not only a chiral order but also the formation of skyrmions in an applied magnetic field. The surface effects in helimagnets and in films with a frustrated surface give rise to the reconstruction of surface spin structure and many striking features due to quantum fluctuations at low T such as the zero-point spin contraction and the magnetization crossover). We have also seen above the surface becomes disordered at a low T while the bulk remains ordered up to a high T. This coexistence of bulk order and surface disorder in a temperature region is also found in several frustrated systems [8].

To conclude, we say that the Green's function theory for non-collinear spin systems is laborious, but it is worth to use it to get results with clear physical mechanisms lying behind observed phenomena in frustrated spin systems.

Acknowledgments: The author thanks his former doctorate students Drs. R. Quartu, C. Santamaria, V. T. Ngo, S. El Hog, A. Bailly-Reyre and I. F. Sharafullin for the collaborative works presented in this review.

Funding: This research received no external funding.

Conflicts of Interest: The authors declare no conflict of interest.

References

1. Zubarev, D. N. Double-time Green Functions in Statistical Physics. *Soviet Physics Uspekhi* **1960**, *3*, 320–345.
2. Diep-The-Hung; Nagai, O.; Levy, J. C. S. Effects of Surface Spin Waves and Surface Anisotropy in Magnetic Thin Films at Finite Temperatures. *Phys. Stat. Sol (b)* **1979**, *93*, 351-361.
3. Yoshimori, A. A New Type of Antiferromagnetic Structure in the Rutile Type Crystal. *J. Phys. Soc. Jpn* **1959**, *14*, 807.
4. Villain, J. La structure des substances magnetiques. *Phys. Chem. Solids* **1959**, *11*, 303.

5. Rastelli, E.; Reatto, L.; Tassi, A. Quantum fluctuations in helimagnets. *J. Phys. C* **1985**, *18*, 353.
6. Diep, H. T. Low-temperature properties of quantum Heisenberg helimagnets. *Phys. Rev. B* **1989**, *40*, 741.
7. Quartu R.; Diep, H. T. Partial order in frustrated quantum spin systems. *Phys. Rev. B* **1997**, *55*, 2975.
8. Diep, H. T.; Giacomini,H. Frustration - Exactly Solved Models. In *Frustrated Spin Systems*; 3rd Edition; Diep, H. T., Editor; World Scientific: Singapore, 2020; pp. 1-60.
9. Dzyaloshinskii, I. E. Thermodynamical Theory of 'Weak" Ferromagnetism in Antiferromagnetic Substances. *Sov. Phys. JETP* **1957**, *5*, 1259.
10. Moriya, T. Anisotropic superexchange interaction and weak ferromagnetism. *Phys. Rev.* **1960**, *120*, 91.
11. Sergienko, A. I.; Dagotto, E. Role of the Dzyaloshinskii-Moriya interaction in multiferroic perovskites. *Phys. Rev. B* **2006**, *73*, 094434.
12. Stashkevich, A.A.; Belmeguenai, M; Roussigné, Y.; Cherif, S.M.; Kostylev, M.; Gabor, M.; Lacour, D.;Tiusan, C.;Hehn, M. Experimental study of spin-wave dispersion in Py/Pt film structures in the presence of an interface Dzyaloshinskii-Moriya interaction. *Phys. Rev. B* **2015**, *91*, 214409.
13. Heide, M.; Bihlmayer, G.; Blügel, S. Dzyaloshinskii-Moriya interaction accounting for the orientation of magnetic domains in ultrathin films: Fe/W(110). *Phys. Rev. B* **2008**, *78*, 140403(R).
14. Ederer, Claude;Spaldin, Nicola A. Weak ferromagnetism and magnetoelectric coupling in bismuth ferrite. *Phys. Rev. B* **2005**, *71*, 060401(R).
15. Cépas, O.; Fong, C. M.; Leung, P. W.;Lhuillier, C. Quantum phase transition induced by Dzyaloshinskii-Moriya interactions in the kagome antiferromagnet. *Phys. Rev. B* **2008**, *78*, 140405(R).
16. Rohart, S.; Thiaville, A. Skyrmion confinement in ultrathin film nanostructures in the presence of Dzyaloshinskii-Moriya interaction. arXiv: 1310.0666 (2013), *Phys. Rev. B* **2013**, *88*184422.
17. Bogdanov, A. N.; Yablonskii, D. A. Thermodynamically stable ?vortics? in magnetically ordered crystals: The mixed state of magnets. *Sov. Phys. JETP* **1989**, *68*, 101.
18. Mühlbauer, S.; Binz, B.; Jonietz, F.; Pfleiderer, C.; Rosch, A.; Neubauer, A.; Georgii, R.; Böni, B. Skyrmion Lattice in a Chiral Magnet. *Science* **2009**, *323*, 915.
19. Yu, X. Z.; Kanazawa, N.; Onose, Y.; Kimoto, K.; Zhang, W. Z.; Ishiwata, S.; Matsui, Y.; Tokura, Y. Near room-temperature formation of a skyrmion crystal in thin-films of the helimagnet FeGe *Nature Mater.* **2011**, *10*, 106.
20. Seki, S.; Yu, X. Z.; Ishiwata, S.; Tokura, Y. Observation of skyrmions in a multiferroic material. *Science* **2012**, *336*, 198.
21. Leonov, A. O.; Mostovoy, M. Multiply periodic states and isolated skyrmions in an anisotropic frustrated magnet. *Nature Communications* **2015**, *6*, 8275.
22. Fert, A.; Cros, V.; Sampaio, J. Skyrmions on the track. *Nature Nanotechnol.* **2013**, *8*, 152.
23. Xia, J.; Zhang, X.; Ezawa, M.; Tretiakov, O. A.; Hou, Z.; Wang, W.; Zhao, G.; Liu, X.; Diep, H. T.; Zhou, Y. Current-driven skyrmionium in a frustrated magnetic system. *Appl. Phys. Lett.* **2020**, *117*, 012403; doi: 10.1063/5.0012706 ; arXiv:2005.01403.
24. Zhang, X.; Xia, J.; Ezawa, M.; Tretiakov, O. A.; Diep, H. T.; Zhao, G.; Liu, X.; Zhou, Y. A Frustrated Bimeronium: Static Structure and Dynamics. *Appl. Phys. Lett.* **2021**, *118*, 052411; doi: 10.1063/5.0034396 ; arXiv:2010.10822v2.
25. Mello, V. D.; Chianca, C. V.; Danta, Ana L.; Carriç, A. S. Magnetic surface phase of thin helimagnetic films. *Phys. Rev. B* **2003**, *67*, 012401.
26. Cinti, F.; Cuccoli, A.; Rettori, A. Exotic magnetic structures in ultrathin helimagnetic holmium films. *Phys. Rev. B* **2008**, *78*, 020402(R).
27. Karhu, E. A.; Kahwaji, S.; Robertson, M. D.; Fritzsche, H.; Kirby,B. J.; Majkrzak, C. F.; Monchesky, T. L. Helical magnetic order in MnSi thin films. *Phys. Rev. B* **2011**, *84*, 060404(R).
28. Karhu, E. A.; Röβler, U. K; Bogdanov, A. N.; Kahwaji, S.; Kirby, B. J.; Fritzsche, H.; Robertson, M. D.; Majkrzak, C. F.; Monchesky, T. L. Chiral modulation and reorientation effects in MnSi thin films. *Phys. Rev. B* **2012**, *85*, 094429.
29. Diep, H. T. Quantum Theory of Helimagnetic Thin Films. *Phys. Rev. B* **2015**, *91*, 014436.
30. Tyablikov, S. V. *Ukr. Mat. Zh.* **1959**, *11*, 289 . Tyablikov, S. VV. *Methods in the Quantum Theory of Magnetism*; Plenum Press: New York, 1967.
31. Diep, H. T. *Theory of Magnetism - Application to Surface Physics*; World Scientific: Singapore, 2013.
32. Bland, J.A.C.; Heinrich, B. (editors),*Ultrathin Magnetic Structures*, vol. I and II; Springer-Verlag: Berlin, 1994.

33. Zangwill, A. *Physics at Surfaces*; Cambridge University Press: London,1988.
34. Diep, H. T. Quantum effects in antiferromagnetic thin films. *Phys. Rev. B* **1991**, *43*, 8509.
35. Diep, H. T. Theory of antiferromagnetic superlattices at finite temperatures. *Phys. Rev. B* **1989**, *40*, 4818.
36. El Hog, S.; Diep, H. T. Helimagnetic Thin Films: Surface Reconstruction, Surface Spin-Waves, Magnetization. *J. Magn. and Magn. Mater.* **2016**, *400*, 276-281.
37. Quartu, R.; Diep, H. T. Phase diagram of body-centered tetragonal helimagnets. *Journal of Magnetism and Magnetic Materials* **1998**, *182*, 38-48.
38. El Hog, S.; Diep, H. T.; Puszkarski, H. Theory of magnons in spin systems with Dzyaloshinskii-Moriya interaction. *J. Phys.: Condens. Matter* **2017**, *29*, 305001. arXiv:1612.04147. hal-01415320 (Dec. 2016).
39. Ngo, V. Thanh; Diep, H. T. Effects of frustrated surface in Heisenberg thin films. *Phys. Rev. B* **2007**, *75*, 035412, Selected for the *Vir. J. Nan. Sci. Tech.* **2007**, *15*, 126.
40. Mermin, N. D.; Wagner, H. Absence of Ferromagnetism or Antiferromagnetism in One- or Two-Dimensional Isotropic Heisenberg Models. *Phys. Rev. Lett.* **1966**, *17*, 1133. Erratum: *17*, 1307.
41. Sharafullin, I. F.; Kharrasov, M. K.; Diep,H. T. Dzyaloshinskii-Moriya interaction in magnetoferroelectric superlattices: Spin waves and skyrmions. *Phys. Rev. B.* **2019**, *99*, 214420.
42. El Hog, S.; Bailly-Reyre, A.; Diep, H. T. Stability and phase transition of skyrmion crystals generated by Dzyaloshinskii-Moriya interaction. *J. Magn. Magn. Mater.* **2018**, *455*, 32–38.
43. Sharafullin, I.F.; Diep, H. T. Skyrmion Crystals and Phase Transitions in Magneto-Ferroelectric Superlattices: Dzyaloshinskii-Moriya Interaction in a Frustrated $J_1 - J_2$ Model. *Symmetry* **2020**, *12*, 26-41.
44. El Hog,S.; Sharafullin, I. F.; Diep, H. T.; Garbouj, H; Debbichi, M.; Said, M. Frustrated Antiferromagnetic Triangular Lattice with Dzyaloshinskii-Moriya Interaction: Ground States, Spin Waves, Skyrmion Crystal, Phase Transition, arXiv2204.12248.
45. Keffer, F. Moriya Interaction and the Problem of the Spin Arrangements in β MnS. *Physical Review* **1962**, *126*, 896.
46. Cheong, S.-W; Mostovoy, M. Multiferroics: a magnetic twist for ferroelectricity. *Nature Materials* **2007**, *6*, 13.
47. Rosales, H. D.; Cabra D. C.; Pujol, P. Three-sublattice Skyrmions crystal in the antiferromagnetic triangular lattice. *Phys. Rev. B* **2015**, *92*, 214439. arXiv:1507.05109v1.
48. Mohylna, M.; Žukovič, M. Stability of skyrmion crystal phase in antiferromagnetic triangular lattice with DMI and single-ion anisotropy. *Journal of Magnetism and Magnetic Materials* **2022**, *546*, 168840.
49. Ngo, V. Thanh; Diep, H. T. Frustration effects in antiferrormagnetic face-centered cubic Heisenberg films. *J. Phys: Condens. Matter.* **2007**, *19*, 386202.
50. Quartu R.; Diep, H. T. Magnetic properties of ferrimagnets. *J. Magnetism and Magnetic Materials* **1997**, *168*, 94-104.
51. Santamaria, C.; Quartu, R.; Diep, H. T. Frustration effect in a quantum Heisenberg spin system. *J. Appl. Phys.* **1998**, *84*, 1953.